Modelled estimates of spatial variability of iron stress in the Atlantic sector of the Southern Ocean

Thomas J. Ryan-Keogh[1,2], Sandy J. Thomalla[1], Thato N. Mtshali[1], Hazel Little[2]

[1]Southern Ocean Carbon and Climate Observatory, Natural Resources and Environment, CSIR, Rosebank, Cape Town 7700, South Africa

[2]Department of Oceanography, University of Cape Town, Rondebosch, Cape Town 7701, South Africa

Correspondence to: Thomas.Ryan-Keogh@uct.ac.za

Abstract

The Atlantic sector of the Southern Ocean is characterized by markedly different frontal zones with specific seasonal and sub-seasonal dynamics. Demonstrated here is the effect of iron on the potential maximum productivity rates of the phytoplankton community. A series of iron addition productivity versus irradiance (PE) experiments utilising a unique experimental design that allowed for 24 hour incubations were performed within the austral summer of 2015/16 to determine the photosynthetic parameters α^B, P^B_{max} and E_k. Mean values for each photosynthetic parameter under iron replete conditions were α^B: 1.46±0.55 (µg (µg Chl a)$^{-1}$ h^{-1} (µM photons m^{-2} s^{-1})$^{-1}$), P^B_{max}: 72.55±27.97 (µg (µg Chl a)$^{-1}$ h^{-1}) and E_k: 50.84±11.89 (µM photons m^{-2} s^{-1}); whereas mean values under the control conditions were α^B: 1.25±0.92 (µg (µg Chl a)$^{-1}$ h^{-1} (µM photons m^{-2} s^{-1})$^{-1}$), P^B_{max}: 62.44±36.96 (µg (µg Chl a)$^{-1}$ h^{-1}) and E_k: 55.81±19.60 (µM photons m^{-2} s^{-1}). There were no clear spatial patterns in either the absolute values or the absolute differences between the treatments at the experimental locations. When these parameters are integrated into a standard depth-integrated primary production model across a latitudinal transect, the effect of iron addition shows higher levels of primary production south of 50°S, with very little difference observed in the sub-Antarctic and Polar Frontal zone. These results emphasize the need for better parameterisation of photosynthetic parameters in biogeochemical models around sensitivities in their response to iron supply. Future biogeochemical models will need to consider the combined and individual effects of iron and light to better resolve the natural background in primary production and predict its response under a changing climate.

1. Introduction

Phytoplankton primary production (PP) in the Southern Ocean is a key contributor to global atmospheric CO_2 drawdown, responsible for 30-40% of global anthropogenic carbon uptake (Khatiwala et al., 2009; Mikaloff Fletcher et al., 2006; Schlitzer, 2002). High nutrient availability fuels this phytoplankton production, but growth is ultimately constrained by the lack of availability of the micronutrient iron (Fe) (de Baar et al., 1990; Martin et al., 1990). This leads to high levels of macronutrients that remain unutilised by phytoplankton growth in what is known as a High Nutrient Low Chlorophyll (HNLC) conditions. Maximum primary productivity rates of the Southern Ocean are also limited by light availability due to low incident solar angles, persistent cloud cover and deep mixed layers that curtail production and subsequently affect the efficiency of the biological carbon pump. Under future climate change scenarios, altered upwelling and mixed layer stratification (Boyd et al., 2001; Boyd and Doney, 2002), changes in sea ice cover (Close and Goosse, 2013; de Lavergne et al., 2014; Montes-Hugo et al., 2008; Zhang, 2007) and food-web dynamics (Dubischar and Bathmann, 1997; Moore et al., 2013; Pakhomov and Froneman, 2004; Smetacek et al., 2004) will alter both the nutrient and light supply strongly impacting primary production rates. As such, it is important that we understand the sensitivity of phytoplankton production to light and micronutrient availability so that we may improve our predictive capability of the response of the Southern Ocean carbon pump to a changing climate.

Iron plays a critical role in modulating PP due to the high requirements of the photosynthetic apparatus, photosystems I and II (Quigg et al., 2003; Raven, 1990; Strzepek and Harrison, 2004; Twining and Baines, 2013). Light availability can further increase the demand for iron, as low irradiance levels increase requirements associated with the synthesis of additional photosynthetic units to increase potential light absorption (Maldonado et al., 1999; Raven, 1990; Strzepek et al., 2012; Sunda and Huntsman, 1997). Iron is also required to activate both nitrate and nitrite reductase (de Baar et al., 2005), which facilitate the assimilation of nitrate and nitrite and their subsequent intracellular reduction to ammonium. In HNLC regions, such as the Southern Ocean, nitrate uptake rates (ρNO_3^-) have also frequently been reported as becoming iron limited (Cochlan, 2008; Lucas et al., 2007; Moore et al., 2013; Price et al., 1994). However, it has also been demonstrated that iron limitation rather than inhibiting nitrate reductase activity results in a bottleneck further downstream due to a reduction in photosynthetically derived reductant (Milligan and Harrison, 2000). This would lead to an excretion of excess nitrate back into the water column that would further contribute to HNLC conditions such as those present in the Southern Ocean.

Estimating PP in the oceans towards an improved understanding of the effects of iron and light limitation requires an understanding of the relationship between photosynthesis (P) and irradiance (E) (Behrenfeld and Falkowski, 1997b; Dower and Lucas, 1993; Platt et al., 2007). PE responses are derived from an equation by Platt et al. (1980), where the responses are parameterized as a function of irradiance. The parameters derived include: P^B_{max}, the biomass-specific rate of photosynthesis at saturating irradiances, α^B, the irradiance-limited biomass-specific initial slope, and E_k, the irradiance at which saturation is initiated. The response of these parameters can be a function of temperature (Behrenfeld and Falkowski, 1997b), but also as a change in the quantum efficiency of photosynthesis, usually as the result of changes in iron availability. In previous iron fertilization experiments a doubling of α^B has been reported (Hiscock et al., 2008), yet this response is not consistent across Southern Ocean waters (Feng et al., 2010; Hopkinson et al., 2007; Moore et al.,

2007; Smith and Donaldson, 2015). Given their relative importance within PP models (Behrenfeld and Falkowski, 1997a, b; Sathyendranath and Platt, 2007), a greater understanding of the drivers of the variability within these photosynthetic parameters is therefore required; particularly if we are to accurately quantify and constrain PP in the Southern Ocean to examine seasonal and interannual variability and trends.

The Atlantic sector of the Southern Ocean is composed of a series of circumpolar fronts that are characterized by large geostrophic velocities (Nowlin and Klinck, 1986; Orsi et al., 1995). The fronts constrain water masses with distinct physical and chemical properties that define different oceanographic zones. These spatial zones, whilst not only displaying zonal variability with the fronts, also display important seasonal contrasts (Thomalla et al., 2011), with differing bloom initiation dates and temporal extent of bloom duration. Whilst the bloom initiation dates can in part be explained by day length and sea ice cover as you move polewards, the differences in the extent and duration of blooms between the zones requires an alternative and more nuanced explanation. One theory that has been postulated is that the supply mechanisms of iron to the mixed layer following the spring bloom varies between zones (Thomalla et al., 2011). Weak diapycnal inputs and a heavy reliance on iron recycling was suggested by Tagliabue et al. (2014) to match approximate phytoplankton utilization within the pelagic zones. An alternative theory that postulates the importance of summer storms may also be pivotal in understanding the seasonal dynamics of phytoplankton primary productivity (Nicholson et al., 2016; Swart et al., 2015; Thomalla et al., 2015), with respect to the sustained bloom observed in the Sub Antarctic Zone (SAZ). Here, summer storms are said to periodically deepen the mixed layer to below the ferricline followed by rapid shoaling during quiescent periods that balances the supply of light and iron in the upper oceans favouring phytoplankton growth that culminates in a sustained summer bloom (Swart et al., 2015). Regardless of the mechanisms at play, an understanding on when and where iron concentrations and supply mechanisms limits potential phytoplankton growth and productivity is needed to better understand the drivers that determine the characteristics of the Southern Ocean seasonal cycle.

To this end, a research cruise was conducted in the austral summer of 2015/16 as part of the third multidisciplinary *Southern Ocean Seasonal Cycle Experiment* (SOSCEx III) which aims to identify and understand the physical and chemical controls on the seasonal cycle of the biological carbon pump. As part of this study, shipboard nutrient addition PE experiments were performed to determine the extent of iron limitation upon phytoplankton primary production.

2. Materials and Methods

2.1. Oceanographic Sampling

The samples and data presented here were obtained during the 55th South African National Antarctic Expedition (3rd December 2015 to 11th February 2016) on-board the S.A. Agulhas II to the Atlantic sector of the Southern Ocean as part of SOSCEx III (Swart et al., 2012). During the cruise, 6 nutrient addition PE long-term experiments were performed within the Atlantic sector of the Southern Ocean (Fig. 1) to determine the extent to which relief from iron limitation could alter the maximal primary productivity rates of the phytoplankton community. Uncontaminated whole seawater was collected from 30-50 m depth using Teflon-lined, external closure 12 L Go-Flo samplers deployed on a trace metal clean CTD rosette system.

2.2. PE Experimental setup

Phytoplankton productivity was measured by the incorporation of ^{13}C stable isotopes in response to an increasing light gradient. Inside a trace metal clean laboratory class-100 container, bulk trace metal clean seawater was decanted unscreened into an acid-washed 50 L LDPE carboy (Thermo scientific) to ensure homogenization; this was then redistributed into acid-cleaned 1.0 L polycarbonate bottles (Nalgene). All experimental conditions were conducted and carried out following trace metal clean standards and conditions. Sample manipulations were conducted under a laminar flow hood. All bottles were inoculated with ^{13}C (10 µM $NaH_2{}^{13}CO_3$/ 100 mL) spikes to achieve an enrichment of ~5%; 11 bottles received the addition of $FeCl_3$ (+2.0 nM, 'Fe'), whereas 11 bottles received the ^{13}C spikes alone ('Control'). The bottles were incubated in screened (LEE Filters) LDPE boxes within light and temperature controlled incubators. Experimental temperature was set to mimic the *in situ* sample collection temperature. Irradiances were measured within the screened boxes using a handheld 4π PAR sensor (Biospherical Instruments) and ranged from 0 – 400 µM photons m^{-2} s^{-1}. Bottles tops were covered with parafilm and double bagged with clear polyethylene bags to minimize contamination risks during the incubation. Due to physical constraints, the experiments were not conducted as triplicates, and as such evaluation of the precision/error within experiments is not possible.

Experiments were incubated for 24 h, after which the samples were vacuum filtered through a pre-combusted (400°C for 24 h) GF/F filter. Samples were acid fumed with concentrated HCl for 24 h to remove inorganic carbon before being dried in an oven at 40°C for 24 h. The isotopic composition of all samples were determined by mass spectrometry on a Flash EA 1112 series elemental analyser (Thermo Finnigan). Carbon uptake rates (µM C h^{-1}) were calculated from the equation of Dugdale and Wilkerson (1986), utilising in situ determinations of dissolved inorganic carbon (DIC). The uptake rates normalised to the chlorophyll-a (Chl) concentration, were used to calculate the maximal light-saturated Chl specific photosynthetic fixation rates (P^B_{max}), the light limited slope (α^B) and the photoacclimation parameter (E_k). The curves and parameters were generated using a non-linear least squares fit to the equation of Platt et al. (1980).

Table 1 Locations for PE experiments conducted during the cruise along with details for the initial chemical, physiological and physical set up conditions.

Experiment	1	2	3	4	5	6
Initiation Date	08/12/2015	05/01/2016	07/01/2016	08/01/2016	09/01/2016	26/01/2016
Latitude (°S)	-42.69	-42.69	-45.99	-50.45	-55.70	-70.44
Longitude (°E/W)	08.74	08.74	05.93	01.04	-00.00	-07.82
Collection Depth (m)	30	35	35	35	50	35
Sunrise: Sunset	03:30 – 18:30	04:00 – 19:00	04:00 – 19:00	04:00 – 19:00	04:00 – 19:00	00:00 – 00:00*
Chl (μg L^{-1})	0.97	0.84	0.89	2.30	1.15	1.49
Nitrate (μM)	7.21	10.20	15.83	21.07	17.02	23.81
Silicate (μM)	0.86	0.72	0.09	3.76	30.83	48.81
Phosphate (μM)	0.88	0.76	0.95	1.28	1.11	0.94
DFe (nM)	0.16	0.17	0.07	0.03	0.05	0.10
F_v/F_m	0.19	0.30	0.35	0.30	0.35	0.37
σ_{PSII} (nm^{-2})	14.79	6.45	5.50	5.59	5.37	3.89
MLD (m)	33.77	56.96	108.42	70.11	42.89	40.80
Salinity	33.87	33.70	33.88	33.80	33.73	33.72
Temp. (°C)	10.80	10.44	6.72	3.17	-1.42	-1.51
Average daytime PAR (μM photons m^{-2} s^{-1})**	1055.31	787.35	289.18	524.41	769.87	673.62
Euphotic Depth (m)	72.79	75.10	52.95	47.92	69.13	78.07

*24 hour day length

**See Sect. 2.7 for details

2.3. Chlorophyll-a and Nutrient Analysis

Samples for Chl analysis, 250 mL, were filtered onto GF/F filters and then extracted into 90% acetone for 24 h in the dark at -20°C, followed by analysis with a fluorometer (TD70; Turner Designs) (Welschmeyer, 1994). Macronutrient samples were drawn into 50 mL diluvials and stored at -20°C until analysis on land. Nitrate + Nitrite and Silicate were measured using a Lachat Flow Injection Analyser (Egan, 2008; Wolters, 2002), whilst Nitrite and Phosphate were determined manually by colorimetric method as specified by Grasshoff et al. (1983). Dissolved iron samples (DFe) were carefully collected in acid-washed 125 mL LDPE bottles, acidified with 30% HCl suprapur to pH ~1.7 (using 2mL L^{-1} criteria) and stored at room temperature until analysis on land at UniBrest in France using the Chemiluminescence – Flow Injection Analyser (CL-FIA) method (Obata et al., 1993). Accuracy and precision of the method was verified by analysis of in-house internal standards and SAFe reference seawater samples (Johnson et al., 2007); the limits of detection were in order of 10 pM.

2.4. Phytoplankton Photosynthetic Physiology

Variable Chl fluorescence was measured using a Chelsea Scientific Instruments FastOcean fast repetition rate fluorometer (FRRf) integrated with a FastAct laboratory system. Samples were acclimated in dark bottles at *in situ* temperatures, and FRRf measurements were blank corrected using carefully prepared 0.2 µm filtrates for all samples (Cullen and Davis, 2003). Protocols for FRRf measurements consisted of the following: 100 x 2 µs saturation flashlets with a 2 µs interval, followed by 25 x 1 µs relaxation flashlets with an interval of 84 µs with a sequence interval of 100 ms. Sequences were repeated 32 times resulting in an acquisition length of 3.2 s. The power of the excitation LED (λ450), was adjusted between samples to saturate the observed fluorescence transients within a given range of $R\sigma_{PSII}$. $R\sigma_{PSII}$, the probability of a reaction centre being closed during the first flashlet, is optimised between 0.042 to 0.064 per the manufacturer specifications. By adopting this approach, it ensures the best signal-to-noise ratio in the recovered parameters whilst accommodating significant variations in the photophysiology of the phytoplankton community without having to adjust the protocol. Data from the FRRf were analysed to derive fluorescence parameters as defined in Baker et al. (2001) and Roháček (2002) by fitting transients to the model of Kolber et al. (1998).

2.5. Pigment Analysis and CHEMTAX

Pigment samples were collected by filtering 0.5 – 2.0 L of water onto GF/F filters. Filters were frozen and stored at -80°C until analysis in Villefranche, France on a HPLC Agilent Technologies 1200. Filters were extracted in 100% methanol, disrupted by sonication, clarified by filtration and analysed by HPLC following the methods of Ras et al. (2008). Limits of detection were on the order of 0.1 ng L^{-1}. Pigment composition data were standardized through root square transformation before cluster analysis utilizing multi-dimensional scaling where similar samples appear together; and dissimilar samples do not. Samples were grouped and analysed in CHEMTAX (Mackey et al., 1996) using the pigment ratios from Gibberd et al. (2013). Multiple iterations of pigment ratios were used to reduce uncertainty in the taxonomic abundance as described in Gibberd et al. (2013), with the solution that had the smallest residual used for the estimated taxonomic abundance.

2.6. Particle Size Analysis

The size distribution of the particle population was measured by running 40 mL of water sample through a 100 µm aperture on a Beckman Coulter-Multisizer (20 runs at 2.0 mL per run), binning the size counts into 400 bins between 2 µm and 60 µm. Data were subsequently analysed utilising custom Matlab scripts to calculate the effective diameter of particles within the sample following Hansen and Travis (1974).

2.7. Depth-integrated Production

Water column primary production rates were calculated according to Platt et al. (1980) and Platt and Sathyendranath (1993) as in Thomalla et al. (2015) where;

$$PP_0 = P_{max} \times (1 - e^{(\frac{-\alpha \times E_0^m \times 0.5}{Pmax})} \quad (1)$$

PP_0 (mg C m^{-2} d^{-1}) is the primary production at the surface, P_{max} the maximal light-saturated photosynthetic fixation rate, α the light-limited slope and E_0^m is daily PAR at the surface, calculated by assuming maximum PAR at midday, zero PAR at sunrise and sunset, a constant gradient of light between time steps and extrapolating the measured PAR (from an above water Biospherical 4π PAR sensor) at the time of the station into an isosceles triangle (see also Thomalla et al. (2015)).

$$E_*^m = \frac{E_0^m}{E_k} \quad (2)$$

The results were generalised by calculating E_*^m(2), the dimensionless daily surface irradiance, while primary productivity over the entire water column PP_{wc} (mg C m^{-2} d^{-1}) was calculated with the following equation (3). The dimensionless function $f(E_*^m)$ for daily primary productivity was solved analytically by Platt et al. (1980). Rates were calculated for both the iron addition and control treatments, allowing the difference between the integrated rates to be solved.

$$PP_{wc} = PP_0 \times \frac{f(E_*^m)}{k_d} \quad (3)$$

K_d was initially calculated as the slope of the natural log of in situ PAR with depth from CTD profiles. When in situ PAR with depth was not available, K_d was also calculated from *in situ* surface Chl concentrations with the following equation (4) (Morel, 1988; Morel et al., 2007). Co-located calculations utilising in situ PAR versus chlorophyll-derived K_d demonstrated on average a 40% higher K_d when calculated with chlorophyll.

$$K_d = 0.0166 + 0.0773 \times [Chl]^{0.6715} \quad (4)$$

2.8. Ancillary physical data

Temperature and salinity profiles were obtained from a Sea-Bird CTD mounted on the rosette system. The mixed layer depth (MLD) was calculated following de Boyer Montégut et al. (2004), which identifies the MLD as the depth where the temperature differs from the temperature at 10 m by more than 0.2°C (ΔT_{10m} = 0.2°C). The position of the fronts was determined using sea surface height (SSH) data from maps of absolute dynamic topography (MADT) according to (Swart et al., 2010).

3. Results

3.1. Oceanographic Context

The experimental set-up locations covered a wide range of pelagic zones from the SAZ to the Marginal Ice Zone (MIZ), each with different physical, chemical and biological properties (see Table 1). Chl concentrations between experiment initiation locations varied between 0.84 – 2.30 µg L^{-1}, peaking just south of the Polar Front at ~50°S. Initial temperatures displayed a characteristic decrease from 10.80°C at the most northerly location to -1.51°C at the MIZ, whereas there were no distinct differences in salinity ranging from 33.70 to 33.88. Macronutrient concentrations all increased polewards, with peaks of 28.15 µM, 1.34 µM and 48.81 µM for nitrate, phosphate and silicate respectively. Dissolved iron concentrations decreased polewards from a maximum of 0.17 nM in the SAZ to minimum values of 0.03 nM and 0.05 nM at 50°S and 55°S respectively, before increasing again in the MIZ to 0.10 nM.

Phytoplankton photophysiology, F_v/F_m, increased polewards from a minimum of 0.19 to a maximum of 0.37, whereas σ_{PSII}, the effective absorption cross-section of PSII, decreased polewards from 14.79 nm^{-2} to 3.89 nm^{-2}. The effective diameter of the phytoplankton population, a relative measure of size, increased polewards from a minimum of 4.29±0.35 µm in the SAZ to a maximum of 8.59±0.68 µm in the MIZ. Estimated taxonomic abundance through HPLC analysis and CHEMTAX determined that the dominant groups at all stations were either Diatoms, Haptophytes or a mix of the two. Haptophytes were the dominant group (>68% of total Chl) in the SAZ during experiments 1 and 2, with Diatoms becoming dominant (>70% of total Chl) from experiment 4 onwards.

MLD's were highly variable and ranged from ~34m at experiment 1 to ~108 m at experiment 3. The MLD was typically deeper than the experimental set up depth (average difference of ~15 m) at all experiments except for experiment 5 where the collection depth was 7 m below the MLD. The CTD density profile at experiment 5 was indicative of 2 mixed layers present, with the experiment performed above the deeper of the mixed layers (~56m). Experiments 1 and 2 that were set up in the same location in the SAZ but 28 days apart had markedly different set up conditions; a 41% increase in the nitrate concentration from 7.21 to 10.20 µM, a two-fold increase in F_v/F_m from 0.19 to 0.35 with a concurrent 56% decrease in σ_{PSII} from 14.79 to 6.45 nm^{-2} and a deepening of the MLD from ~34 m to ~57 m.

The light environment within the water column at each location was determined by calculating the percentage light depth as a function of the vertical attenuation coefficient of irradiance (K_d). The percentage light depths of the experiments ranged between 3.46% to 14.78%. The 1% light depth, which typically coincides with the compensation light depth i.e. the depth where rates of production equate to rates of respiration, is consistently below the MLD, except for experiment 4 where it was 22 m above the mixed layer.

3.2. PE Parameters

PE curves for carbon uptake (ρC) (Fig. 2, Fig. S1), summarised in Table 2, display consistent results with greater values of α^B and P^B_{max} with the addition of iron compared to the control treatments (Fig. S2, Fig. S3). The PE curves for the control treatments did not display any significant outliers (r^2 = >95%), we can assume

that contamination levels were minimal; as no measurements of dFe in the sample bottles were collected. The values derived here fall within the range previously reported for iron addition experiments in the Southern Ocean (Hiscock et al., 2008; Hopkinson et al., 2007; Moore et al., 2007; Smith and Donaldson, 2015). Maximum values of α^B (mg C (mg Chl a)$^{-1}$ h^{-1} (µmol photons m^{-2} s^{-1})$^{-1}$) for ρC were 2.23 x 10^{-3} from experiment 2 Fe treatment and 2.43 x 10^{-3} from experiment 1 control treatment, with minimum values of 0.13 x 10^{-3} from experiment 5 control treatment and 0.56 x 10^{-3} from experiment 6 Fe treatment. P^B_{max} (mg C (mg Chl a)$^{-1}$ h^{-1}) values peaked in experiment 1 Fe treatment, with a minimum value of 1.06 x 10^{-2} in experiment 5 control treatment. E_k (µmol photons m^{-2} s^{-1}) peaked at 79.77, with minimum values in experiment 1 control treatment. Despite the substantial differences in set up conditions for experiments 1 and 2 in the SAZ, occupied twice over the space of 28 days, there were no significant differences in the responses of the PE parameters to Fe. Due to constraints in light levels for the incubator set up, light levels that may result in photoinhibition (>400 µmol photons m^{-2} s^{-1}) were not achieved and as such no measurements of β were determined.

To better understand the effects of iron limitation on the PE parameters, the absolute differences (Fig. 3) of α^B, P^B_{max}, and E_k between the iron treatments and control treatments were calculated. $\Delta\alpha^B$ ranged from -6.94 x 10^{-4} to 1.30 x 10^{-3}, with minimum and maximum percentage differences of -40.04% and 91.12% respectively. ΔP^B_{max} ranged between 4.98 x 10^{-2} and -1.02 x 10^{-2}, with minimum and maximum percentage differences of -12.10% and 82.52%; the greatest value for ΔE_k was -40.92 for experiment 5. Maximal values of all differences were consistently found in experiment 5 which was set up just south of the Southern Boundary front (Figure 3).

Table 2 Summary of PE parameters, α^B (mg (mg Chl a)$^{-1}$ h^{-1} (µmol photons m^{-2} s^{-1})$^{-1}$), P^B_{max} (mg (mg Chl a)$^{-1}$ h^{-1}) and E_k (µmol photons m^{-2} s^{-1}), for the ρC nutrient addition experiments.

	Experiment	**1**	**2**	**3**	**4**	**5**	**6**
ρC	α^B $_{(Fe)}$ (x 10^{-3})	1.73	2.23	1.23	1.56	1.43	0.56
	α^B $_{(Control)}$ (x 10^{-3})	2.43	2.16	1.19	1.21	0.13	0.37
	$P^B_{max(Fe)}$ (x 10^{-2})	10.67	9.30	8.46	6.22	6.04	2.86
	$P^B_{max(Control)}$ (x 10^{-2})	9.23	9.14	9.48	5.99	1.06	2.56
	$E_{k\ (Fe)}$	61.52	41.72	68.59	39.80	42.29	51.12
	$E_{k\ (Control)}$	38.03	42.40	79.77	49.46	83.21	69.37

Potential drivers of variability within the photosynthetic parameters were determined through a Pearson's linear correlation coefficient matrix (Fig. 4), revealing significant negative and positive relationships with sea surface temperature (SST), salinity, nitrate and silicate concentrations, photosynthetic physiology parameters (F_v/F_m and σ_{PSII}) as well as measures of the community structure; effective diameter and ratio of Diatoms to Haptophytes. There were no significant relationships with either dissolved iron concentrations or chlorophyll concentrations.

Other parameters that did not show any relationships and were excluded from the matrix include MLD, the light environment (*in situ* PAR and 1% light depth) and phosphate concentrations. α^B for the control treatments displayed the greatest number of relationships with SST, nitrate concentrations, community structure variables and F_v/F_m. The relative differences in all the parameters showed strong positive correlations with SST and salinity ($p<0.05$). A principle component analysis (PCA) was carried out on the data with the variables' PCA projection on the factor plane represented in Fig. S4. The sum of the first two PC's explained 76.74% of the total variance. The factor plane representation splits the variables, both experimental and initial conditions, into the four different quadrants. The grouping of the variables within each quadrant agree with the positive correlations determined within the correlation coefficient matrix; whereas variables in opposite quadrants agree with the negative correlations.

3.3. Primary Production

Depth integrated primary production (PP_{wc}) was calculated at each experimental location and displayed a wide range of variability with and without iron (Fig. 5). On average PP_{wc} was higher in the iron addition treatments (Fig. 5a); with an average of 387.32 ± 207.18 (mg C m^{-2} d^{-1}) for iron addition and an average of 315.37 ± 229.37 (mg C m^{-2} d^{-1}) for the control. The maximum absolute differences in PP_{wc} (ΔPP_{wc}, Fig. 5b) of 228.82 mc C m^{-2} s^{-1} was found in experiments 5 at ~55°S near the Southern Boundary front, with very little difference observed in ΔPP_{wc} at experiments 3 and 4.

The responses of Fe addition to primary production from the 6 experiments were extrapolated onto broader spatial and temporal scales, whereby underway measurements of Chl were converted into K_d using equation 4. This, when combined with underway measurements of surface PAR allowed us to look at latitudinal gradients in primary production (as per equations 1, 2 and 3). As the PE parameters displayed strong linear correlations with latitude, (α R^2 = 0.73 and 0.66, P_{max} R^2 = 0.91 and 0.68 for Fe and Control respectively), a linear interpolation was applied to P_{max} and α extrapolating the values from 6 points to a 0.1° resolution along the cruise track. The interpolated values of P_{max} and α were combined with underway measurements of K_d and PAR to calculate PP_{wc} with and without Fe addition for the three different occupations of the same transect line (Fig. 6a). A high degree of variability was revealed between occupations in the SAZ and polar frontal zone (PFZ) but no clear differences between the iron and control treatments. Variability in the SAZ and PFZ appears to be temporally driven, with higher values of PP_{wc} found in the third occupation of the transect line later in the summer season. Differences in PP_{wc} between the two treatments become evident south of 50°S (Fig. 6a and 6b), with all three iron treatment occupations being ~0.5 g C m^{-2} d^{-1} higher than their control treatment counterparts. The differences between the control and Fe treatments were calculated for each transect, which when combined allowed for the calculation of an average absolute difference in primary productivity (ΔPP_{wc}, Fig. 6c). ΔPP_{wc} is slightly negative within the SAZ and PFZ, before sharply increasing to a maximum difference of 0.85 g C m^{-2} d^{-1} at 58°S. ΔPP_{wc} begins to decrease with increasing latitude before reaching an average difference of 0.11 g C m^{-2} d^{-1} in the MIZ. Representing these differences in PP_{wc} as a percentage difference (Fig. 6d) shows that within the SAZ, PFZ and MIZ the differences are ±10-20%; whereas within the Antarctic zone (55°S–65°S) the differences between the treatments can be as much as 80%.

Given the limitations of our data set (that requires the use of interpolated values of P_{max} and α) together with the weight we place on the conversion of these parameters to PP (with chlorophyll and PAR), it is important that we understand the sensitivity of the PP model to variability in the different input parameters. To test this, we performed a series of sensitivity tests to determine which components present the greatest influence on the final PP values. The sensitivity tests were divided into the three components of the equation; K_d derived from chlorophyll (Fig. S5), surface PAR (Fig. S6) and the photosynthetic parameters (P_{max} and α) (Fig. S7). For consistency, the range of variation for each parameter was calculated and used as a factor to alter each component. The mean range of variability for Kd was 84.33%, surface PAR was 68.73%, and α and P_{max} were 82.85% and 83.01% respectively. If K_d values are increased by 84.33% this results in a 29.61% decrease in ΔPP_{wc}, whereas a decrease of K_d results in an increase in ΔPP_{wc}, of 59.17%. Increasing surface PAR resulted in an increase in ΔPP_{wc} of 3.50%; whilst decreasing PAR corresponded to a decrease of 8.06%. The largest differences in ΔPP_{wc} were generated when P_{max} was altered by 83.01%, in accordance with the range of variability, resulting in an increase of 42.97% and a decrease of 80.92% in ΔPP_{wc} (for an increase and decrease in P_{max} respectively). The other PE parameter, α, did not result in the same level of changes in ΔPP_{wc} and only increased by 4.01% and decreased by 12.22% for an increase and decrease in α by 82.85% respectively.

4. Discussion

Phytoplankton biomass in the Southern Ocean is potentially limited in their extent and magnitude predominantly by the availability of the micronutrient iron (Blain et al., 2007; Boyd et al., 2000; Pollard et al., 2009). This conclusion is based on the combination of two factors, the high iron requirements for photosynthetic proteins (Quigg et al., 2003; Raven, 1990; Strzepek and Harrison, 2004; Twining and Baines, 2013) and the lack of supply sources of iron to the Southern Ocean (Duce and Tindale, 1991; Tagliabue et al., 2014). The result of which is an environment that displays high degrees of spatial and temporal variability in primary production in response to highly variable iron supply mechanisms that result in chlorophyll patchiness (Fig. 1) and a complex seasonality (Thomalla et al., 2011). Iron limitation is potentially strongest during the summer months when light levels are not considered limiting (Boyd et al., 2010) and the spring bloom is expected to have utilised the bulk of the winter iron resupply. In the austral summer of 2015/2016 a series of iron addition photosynthesis versus irradiance experiments were performed in the Atlantic Southern Ocean to determine the extent to which iron availability was limiting maximal rates of primary productivity.

The addition of iron appeared to stimulate increased productivity to varying degrees (Fig. 2, Fig. 3b, Fig. S1, Fig. S2, Fig. S3) with average P_{max} and α values being higher for an iron replete system (12.75±6.95 and 0.25±0.14) compared to a control system (11.17±8.23 and 0.22±0.19), suggestive that iron is indeed a micronutrient limiting phytoplankton production in this region. Similar responses have been reported by Hiscock et al. (2008) under conditions of sub-saturating light conditions, where the addition of iron can result in a doubling of photosynthetic rates. However, a nutrient addition PE experiment in the Ross Sea demonstrated no significant increases in α^B or P^B_{max} (Smith and Donaldson, 2015). One potential reason for this is the length of their incubation period, which was only 2 hours and may not have been enough for the phytoplankton to incorporate the iron into their photosynthetic proteins and produce higher productivity rates. Indeed, nutrient addition experiments performed under similar conditions were shown to require 24 hours to see any significant differences in initial changes in photophysiology (Browning et al., 2014; Ryan-Keogh et al., 2017; Ryan-Keogh et al., 2013) with changes in biomass only being reported after 48 hours. This shortcoming highlights the attraction of the unique experimental design utilised here, which allows for 24-hour Fe addition and control incubations at varying light levels and constant temperature. However, it should be noted that a time-length of 24 hours may not be sufficient to complete alleviate the iron-mediated photosynthetic response and as such these results may only reflect initial responses rather than longer term community level responses to relief from iron limitation. It should be noted however, that light acclimation can between 2 – 6 hours and as such be reflected in the potential iron demand, a lower demand at higher irradiances (Strzepek et al., 2012). Such incidences would impact the observed differences between PE parameters in control versus Fe addition experiments. However, since the light range of the experiments (0 – 400) fall below the maximum light intensities measured *in situ* (Table 1), acclimation responses are unlikely to dominate and indeed if occurring would result in an underestimation of the differences between control and addition experiments. The experimental design of 24 hours, whilst suitable for investigating iron limitation, means that results are not truly representative of *in situ* photosynthetic parameters and should not be interpreted as such.

Potential factors that are known to be associated with iron-induced enhanced primary productivity include temperature, macronutrient concentrations, Chl, MLD, light history and community composition. A

Pearson's linear correlation matrix (Fig. 4) was carried out on an array of variables to examine the influence of key physical, chemical and biological factors on the variability of photosynthetic parameters in this study. Significant relationships were found with SST, salinity and macronutrient concentrations, which show strong latitudinal gradients. A proxy for the community structure that utilized the ratio of the 2 dominant groupings (Diatoms and Haptophytes) also indicated strong significant relationships with the PE parameters, which is potentially driven by Si availability controlling community structure. Indeed, it has been demonstrated that in the SAZ, where haptophytes dominated during this study, there is evidence for Fe-Si co-limitation. In a study by Hutchins et al. (2001) it was demonstrated that the addition of both Fe and Si resulted in the greatest responses in chlorophyll and the photosynthetic parameters. The relationship here may not be driven by Fe availability on the PE parameters, but rather community level limitation. No significant relationships were however found between PE parameters and iron or Chl concentrations. The lack of significant relationships could be due to the small range of variability observed in these parameters; for example, Chl concentrations at all stations were typically low (0.84 – 2.30 (μg L^{-1}) when compared to the range of chlorophyll concentrations measured throughout the entire cruise (0.01 – 11.25 μg L^{-1}). The lack of a relationship with dissolved iron concentrations highlights how this proxy is not necessarily a good indicator of iron stress, as any limiting nutrient would be expected to be severely depleted by biological uptake with a resultant ambient concentration that would remain close to zero despite possible event scale supply (Ryan-Keogh et al., 2017).

The photosynthetic parameters derived here are important components in a suite of models that derive estimates of phytoplankton primary production (Behrenfeld and Falkowski, 1997a, b; Sathyendranath and Platt, 2007). Different primary production models inherently consist of certain biases towards modelling the photosynthetic parameters whereas others have excluded them entirely from the computation of primary productivity rates. Hiscock et al. (2008) demonstrated that the variables in the Behrenfeld and Falkowski (1997b) standard depth-integrated model (DIM) exerted considerably different forcing mechanisms on the final primary productivity rates. In the case of this DIM, phytoplankton biomass was the dominant variable that could result in three orders of magnitude changes in primary production, compared to only a 40-fold change when altering the photosynthetic parameter P^B_{opt} (i.e. P^B_{max}). This highlights the need to understand the sensitivity of different PP models to variability within their input parameters.

Results from the production model applied here (equations 1, 2 and 3) show a general decrease with latitude in depth-integrated primary production (PP_{wc}), with significant differences between treatments (t-test, $p<0.05$). One station near the Southern Boundary exhibited the greatest differences in ΔPP_{wc} with a value of 0.89 g C m^{-2} d^{-1} (Fig. 5b), with the lowest observed ΔPP_{wc} of 0.11 g C m^{-2} d^{-1} south of the polar front. The low sampling frequency of the experiments both spatially and temporally (6 experiments spanning two months and the entire latitudinal extent of the Southern Ocean) together with the diverse range of initial set up conditions (Table 1) make it difficult to interpret the causal relationships observed within each experiment with any certainty. Instead, the information from these experiments were maximised through an alternate approach that utilised the range of variability in PE parameters in control versus iron addition experiments to gain a broader spatial interpretation of the response of phytoplankton production to iron addition.

A linear interpolation of the PE parameters (P_{max} and α) with latitude, together with underway measurements of PAR and K_d (derived from surface Chl) allow for the generation of high resolution rates of PP_{wc} with and without Fe addition for three occupations of the cruise transect (Fig. 6a). Within the SAZ and

PFZ there was a high degree of variability between the three occupations, with higher PP_{wc} values later in the growing season (Fig. 6a). However, there were no clear differences between the iron and control treatments in any of the occupations. This may not reflect a lack of iron limitation in the SAZ, as it has been demonstrated previously that there is ecological and physiological iron limitation (Coale et al., 2004), with longer experiments demonstrating increases in P_{max} and α following iron addition (Hutchins et al., 2001). Whereas south of 50°S there were no differences as the growing season progressed but a clear difference between the iron and control treatments (Fig. 6b and 6c). Here, a maximum percentage difference of ~80% (Fig. 6d) was observed between control and iron replete conditions, with ΔPP_{wc} peaking at 0.85 g C m^{-2} y^{-1} at 55°S. Differences between iron addition and control systems begin to decline within the MIZ (Fig. 6c). These results suggest that there are potential differences in iron availability and supply within different zones of the Southern Ocean, which agrees with previous studies which postulated that the bloom extent and duration within the SAZ could potentially be driven by enhanced iron supply through storm-eddy interaction (Nicholson et al., 2016) while in the MIZ addition iron is supplied through melting ice (Gao et al., 2003; Grotti et al., 2005; Sedwick and DiTullio, 1997). The Fe addition test performed here demonstrates the sensitivity of waters south of 50°S to Fe availability, if models do not consider this sensitivity then the degree of error for PP models can be as high as 80%. It must be noted that the transects will not only reflect latitudinal gradients but will also contain a seasonal signal as the cruise spanned 2 months across the austral summer. A seasonal shift in community structure of haptophytes increasing their dominance beyond the SAZ into the PFZ was evident from underway measurements of community structure (data not shown); indicative of seasonal Si limitation for this region (Boyd et al., 2010). Moreover, the complex seasonality of this region represents shifts between varying co-limitations that will be represented not only in the PE parameters measured, but also in the additional components utilized to calculate PP_{wc}.

From these results, it became clear that higher values of P_{max} and α because of iron addition were significantly influencing the model outputs of primary production. However, the extent to which changes in the PE parameters were responsible for the latitudinal trend in ΔPP_{wc} versus changes in ancillary parameters (e.g. Chl, PAR) is unclear. To test our interpretation of the variability in PP_{wc} being a direct response to Fe availability through changes in the PE parameters, a series of sensitivity analyses were performed which showed that PAR and α exerted very little influence (Fig. S6 and S7). Biomass (Chl), as represented through K_d, did exert a large influence on PP_{wc} (up to 59%, Fig. S5), but this influence could be overestimated due to potential errors in the calculation of K_d (Morel et al., 2007). However the greatest influence was P_{max} (up to 81%, Fig. S7). As such, we can conclude that the primary driver of the latitudinal trend in ΔPP_{wc} is the result of changes in the maximum photosynthetic capacity (P_{max}) to iron addition, however regions along the transect may be experiencing seasonal co-limitation of Fe and Si, particularly during the third transect conducted during late summer.

The photosynthetic parameters P_{max} and α remain difficult to fully parameterise due to interacting effects of iron, light availability, temperature and community structure, yet these parameters remain critical components of different biogeochemical models. Our results show that if models fail to capture the interacting effects of iron and other parameters on primary productivity, then the degree of error across vast extents of the Southern Ocean can be significant (as much as 80%). On the other hand, any model that can correctly account for variability in these parameters will better reproduce the natural background levels of primary productivity

and the seasonal cycle for application to iron limited areas of the ocean including the Sub-Arctic Pacific and the Southern Ocean.

Acknowledgements

We would like to thank the South African National Antarctic Programme (SANAP) and the captain and crew of the SA Agulhas II for their professional support throughout the cruise. Ryan Cloete and Ryan Miltz were involved in experimental set up; Natasha van Horsten and Warren Joubert performed the DIC determinations for calculation of carbon assimilation. This work was undertaken and supported through the CSIR's Southern Ocean Carbon and Climate Observatory (SOCCO) Programme (http://socco.org.za/). This work was supported by CSIR's Parliamentary Grant funding and the NRF SANAP grant (SNA14073184298).

References

Baker, N. R., Oxborough, K., Lawson, T., and Morrison, J. I. L.: High resolution imaging of photosynthetic activities of tissues, cells and chloroplasts in leaves, J Exp Bot, 52, 615-621, 10.1093/jexbot/52.356.615, 2001.

Behrenfeld, M. J. and Falkowski, P. G.: A consumer's guide to phytoplankton primary productivity models, Limnol Oceanogr, 42, 1479-1491, 10.4319/lo.1997.42.7.1479, 1997a.

Behrenfeld, M. J. and Falkowski, P. G.: Photosynthetic rates derived from satellite-based chlorophyll concentration, Limnol Oceanogr, 42, 1-20, 10.4319/lo.1997.42.1.0001, 1997b.

Blain, S., Queguiner, B., Armand, L., Belviso, S., Bombled, B., Bopp, L., Bowie, A., Brunet, C., Brussaard, C., Carlotti, F., Christaki, U., Corbiere, A., Durand, I., Ebersbach, F., Fuda, J. L., Garcia, N., Gerringa, L., Griffiths, B., Guigue, C., Guillerm, C., Jacquet, S., Jeandel, C., Laan, P., Lefevre, D., Lo Monaco, C., Malits, A., Mosseri, J., Obernosterer, I., Park, Y. H., Picheral, M., Pondaven, P., Remenyi, T., Sandroni, V., Sarthou, G., Savoye, N., Scouarnec, L., Souhaut, M., Thuiller, D., Timmermans, K., Trull, T., Uitz, J., van Beek, P., Veldhuis, M., Vincent, D., Viollier, E., Vong, L., and Wagener, T.: Effect of natural iron fertilization on carbon sequestration in the Southern Ocean, Nature, 446, 1070-1074, 10.1038/nature05700, 2007.

Boyd, P. W., Crossely, A. C., DiTullio, G. R., Griffiths, F. B., Hutchins, D. A., Queguiner, B., Sedwick, P. N., and Trull, T. W.: Control of phytoplankton growth by iron supply and irradiance in the subantarctic Southern Ocean: Experimental results from the SAZ Project, J Geophys Res, 106, 31573-31583, 10.1029/2000JC000348, 2001.

Boyd, P. W. and Doney, S. C.: Modelling regional responses by marine pelagic ecosystems to global climate change, Geophysical Research Letters, 29, 10.1029/2001GL014130, 2002.

Boyd, P. W., Strzepek, R., Fu, F. X., and Hutchins, D. A.: Environmental control of open-ocean phytoplankton groups: Now and in the future, Limnol Oceanogr, 55, 1353-1376, 10.4319/lo.2010.55.3.1353, 2010.

Boyd, P. W., Watson, A. J., Law, C. S., Abraham, E. R., Trull, T., Murdoch, R., Bakker, D. C. E., Bowie, A. R., Buesseler, K. O., Chang, H., Charette, M., Croot, P., Downing, K., Frew, R., Gall, M., Hadfield, M., Hall, J., Harvey, M., Jameson, G., LaRoche, J., Liddicoat, M., Ling, R., Maldonado, M. T., McKay, R. M., Nodder, S., Pickmere, S., Pridmore, R., Rintoul, S., Safi, K., Sutton, P., Strzepek, R., Tanneberger, K., Turner, S., Waite, A., and Zeldis, J.: A mesoscale phytoplankton bloom in the polar Southern Ocean stimulated by iron fertilization, Nature, 407, 695-702, 10.1038/35037500, 2000.

Browning, T. J., Bouman, H. A., Moore, C. M., Schlosser, C., Tarran, G. A., Woodward, E. M. S., and Henderson, G. M.: Nutrient regimes control phytoplankton ecophysiology in the South Atlantic, Biogeosciences, 11, 463-479, 10.5194/bg-11-463-2014, 2014.

Close, S. E. and Goosse, H.: Entrainment-driven modulation of Southern Ocean mixed layer properties and sea ice variability in CMIP5 models, Journal of Geophysical Research-Oceans, 118, 2811-2827, 10.1002/jgrc.20226, 2013.

Coale, K. H., Johnson, K. S., Chavez, F. P., Buesseler, K. O., Barber, R. T., Brzezinski, M. A., Cochlan, W. P., Millero, F. J., Falkowski, P. G., Bauer, J. E., Wanninkhof, R. H., Kudela, R. M., Altabet, M. A., Hales, B. E., Takahashi, T., Landry, M. R., Bidigare, R. R., Wang, X., Chase, Z., Strutton, P. G., Friederich, G. E., Gorbunov, M. Y., Lance, V. P., Hilting, A. K., Hiscock, M. R., Demarest, M., Hiscock, W. T., Sullivan, K. F., Tanner, S. J., Gordon, R. M., Hunter, C. N., Elrod, V. A., Fitzwater, S. E., Jones, J. L., Tozzi, S., Koblizek, M.,

Roberts, A. E., Herndon, J., Brewster, J., Ladizinsky, N., Smith, G., Cooper, D., Timothy, D., Brown, S. L., Selph, K. E., Sheridan, C. C., Twining, B. S., and Johnson, Z. I.: Southern Ocean Iron Enrichment Experiment: Carbon Cycling in High- and Low-Si Waters, Science, 304, 408-414, 2004.

Cochlan, W. P.: Nitrogen Uptake in the Southern Ocean. In: Nitrogen in the Marine Environment, Elsevier, Amsterdam, 2008.

Cullen, J. J. and Davis, R. F.: The blank can make a big difference in oceanographic measurements, Limnology and Oceanography Bulletin, 12, 29-35, 10.1002/lob.200312229, 2003.

de Baar, H. J. W., Boyd, P. W., Coale, K. H., Landry, M. R., Tsuda, A., Assmy, P., Bakker, D. C. E., Bozec, Y., Barber, R. T., Brezinski, M. A., Buesseler, K. O., Boyé, M., Croot, P. L., Gervais, F., Gorbunov, M. Y., Harrison, P. J., Hiscock, W. T., Laan, P., Lancelot, C., Law, C. S., Levasseur, M., Marchetti, A., Millero, F. J., Nishioka, J., Nojiri, Y., van Oijen, T., Riebesell, U., Rijkenberg, M. J. A., Saito, H., Takeda, S., Timmermans, K. R., Veldhuis, M. J. W., Waite, A. M., and Wong, C. S.: Synthesis of iron fertilization experiments: From the iron age in the age of enlightenment, J Geophys Res, 110, C09S16, 10.1029/2004JC002601, 2005.

de Baar, H. J. W., Buma, A. G. J., Nolting, R. F., Cadee, G. C., Jacques, G., and Treguer, P. J.: On iron limitation of the Southern Ocean: Experimental observations in the Weddell and Scotia Seas, Mar Ecol Prog Ser, 65, 105-122, 1990.

de Boyer Montégut, C., Madec, G., Fischer, A. S., Lazar, A., and Iudicone, D.: Mixed layer depth over the global ocean: an examination of profile data and a profile-based climatology, J Geophys Res, 109, C12003, 10.1029/2004JC002378, 2004.

de Lavergne, C., Palter, J. B., Galbraith, E. D., Bernardello, R., and Marinov, I.: Cessation of deep convection in the open Southern Ocean under anthropogenic climate change, Nature Climate Change, 4, 278-282, 10.1038/nclimate2132, 2014.

Dower, K. M. and Lucas, M. I.: Photosynthesis-irradiance relationships and production associated with a warm-core ring shed from the Agulhas Retroflection south of Africa, Mar Ecol Prog Ser, 95, 141-154, 10.3354/meps095141, 1993.

Dubischar, C. D. and Bathmann, U. V.: Grazing impacts of copepods and salps on phytoplankton in the Atlantic sector of the Southern Ocean, Deep-Sea Research II, 44, 415-433, 10.1016/S0967-0645(96)00064-1, 1997.

Duce, R. A. and Tindale, N. W.: Atmospheric Transport of Iron and Its Deposition in the Ocean, Limnol Oceanogr, 36, 1715-1726, 10.4319/lo.1991.36.8.1715, 1991.

Dugdale, R. C. and Wilkerson, F. P.: The use of 15N to measure nitrogen uptake in eutrophic oceans; experimental considerations, Limnol Oceanogr, 31, 673-689, 10.4319/lo.1986.31.4.0673, 1986.

Egan, L.: QuickChem Method 31-107-04-1-C - Nitrate and/or Nitrite in brackish or seawater, Lachat Instruments, 2008.

Feng, Y., Hare, C. E., Rose, J. M., Handy, S. M., DiTullio, G. R., Lee, P. A., Smith, W. O., Jr., Peloquin, J., Tozzi, S., Sun, J., Zhang, Y., Dunbar, R. B., Long, M. C., Sohst, B., Lohan, M., and Hutchins, D. A.: Interactive effects of iron, irradiance and CO_2 on Ross Sea phytoplankton, Deep-Sea Research I, 57, 368-383, 10.1016/j.dsr.2009.10.013, 2010.

Gao, Y., Fan, S.-M., and Sarmiento, J. L.: Aeolian iron input to the ocean through precipitation scavenging: A modeling perspective and its implication for natural iron fertilization in the ocean, J Geophys Res, 108, 10.1029/2002JD002420, 2003.

Gibberd, M.-J., Kean, E., Barlow, R., Thomalla, S., and Lucas, M.: Phytoplankton chemotaxonomy in the Atlantic sector of the Southern Ocean during late summer 2009, Deep-Sea Research I, 78, 70-78, 10.1016/j.dsr.2013.04.007, 2013.

Grasshoff, K., Ehrhardt, M., and Kremling, K.: Methods of seawater analysis, Verlag Chemie, Wienheim, Germany, 1983.

Grotti, M., Soggia, F., Ianni, C., and Frache, R.: Trace metals distributions in coastal sea ice of Terra Nova Bay, Ross Sea, Antarctica, Antarct Sci, 17, 289-300, 2005.

Hansen, J. E. and Travis, L. D.: Light scattering in planetary atmospheres, Space Science Reviews, 16, 527-610, 10.1007/BF00168069, 1974.

Hiscock, M. R., Lance, V. P., Apprill, A. M., Johnson, Z., Bidigare, R. R., Mitchell, B. G., Smith, W. O. J., and Barber, R. T.: Photosynthetic maximum quantum yield increases are an essential component of Southern Ocean phytoplankton iron response, Proc Natl Acad Sci U S A, 105, 4775-4780, 10.1073/pnas.0705006105, 2008.

Hopkinson, B. M., Mitchell, B. G., Reynolds, R. A., Wang, H., Selph, K. E., Measures, C. I., Hewes, C. D., Holm-Hansen, O., and Barbeau, K. A.: Iron limitation across chlorophyll gradients in the southern Drake Passage: Phytoplankton responses to iron addition and photosynthetic indicators of iron stress, Limnol Oceanogr, 52, 2540-2554, 10.4319/lo.2007.52.6.2540, 2007.

Hutchins, D. A., Sedwick, P. N., DiTullio, G. R., Boyd, P. W., Quéguiner, B., Griffiths, F. B., and Crossely, C.: Control of phytoplankton growth by iron and silicic acid availability in the subantarctic Southern Ocean: Experimental results from the SAZ Project, J Geophys Res, 106, 31559-31572, 10.1029/2000JC000333, 2001.

Johnson, K. S., Elrod, V. A., Fitzwater, S. E., Plant, J., Boyle, E., Bergquist, B., Bruland, K. W., Aguilar-Islas, A. M., Buck, K., Lohan, M. C., Smith, G. J., Sohst, B. M., Coale, K. H., Gordon, M., Tanner, S., Measures, C. I., Moffett, J., Barbeau, K. A., King, A., Bowie, A. R., Chase, Z., Cullen, J. J., Laan, P., Landing, W., Mendez, J., Milne, A., Obata, H., Doi, T., Ossiander, L., Sarthou, G., Sedwick, P. N., Van den Berg, S., Laglera-Baquer, L., Wu, J.-F., and Cai, Y.: Developing standards for dissolved iron in seawater, Eos, Transactions American Geophysical Union, 88, 131-132, 10.1029/2007EO110003, 2007.

Khatiwala, S., Primeua, F., and Hall, T.: Reconstruction of the history of anthropogenic CO_2 concentrations in the ocean, Nature, 462, 346-349, 10.1038/nature08526, 2009.

Kolber, Z. S., Prášil, O., and Falkowski, P. G.: Measurements of variable chlorophyll fluorescence using fast repetition rate techniques: defining methodology and experimental protocols, Biochim Biophys Acta, 1367, 88-106, 10.1016/S0005-2728(98)00135-2, 1998.

Lucas, M., Seeyave, S., Sanders, R., Moore, C. M., Williamson, R., and Stinchcombe, M.: Nitrogen uptake responses to a naturally Fe-fertilised phytoplankton bloom during the 2004/2005 CROZEX study, Deep-Sea Research II, 54, 2138-2173, 10.4319/lo.2007.52.6.2540, 2007.

Mackey, M. D., Mackey, D. J., Higgins, H. W., and Wright, S. W.: CHEMTAX - a program for estimating class abundances from chemical markers: application to HPLC measurements of phytoplankton, Mar Ecol Prog Ser, 144, 265-283, 10.3354/meps144265, 1996.

Maldonado, M. T., Boyd, P. W., Harrison, P. J., and Price, N. M.: Co-limitation of phytoplankton growth by light and Fe during winter in the NE subarctic Pacific Ocean, Deep-Sea Research II, 46, 2475-2485, 10.1016/S0967-0645(99)00072-7, 1999.

Martin, J. H., Gordon, R. M., and Fitzwater, S. E.: Iron in Antarctic waters, Nature, 345, 156-158, 10.1038/345156a0, 1990.

Mikaloff Fletcher, S. E., Gruber, N., Jacobson, A. R., Doney, S. C., Dutkiewicz, S., Gerber, M., Follows, M., Joos, F., Lindsay, K., Menemenlis, D., Mouchet, A., Müller, S. A., and Sarmiento, J. L.: Inverse estimates of anthropogenic CO_2 uptake, transport, and storage by the the ocean, Global Biogeochemical Cycles, 20, GB2002, 10.1029/2005GB002530, 2006.

Milligan, A. J. and Harrison, P. J.: Effects of non-steady-state iron limitation on nitrogen assimilatory enzymes in the marine diatom Thalassiosira weissflogii (Bacillariophyceae), J Phycol, 36, 78-86, 10.1046/j.1529-8817.2000.99013.x, 2000.

Montes-Hugo, M., Doney, S. C., Ducklow, H. W., Fraser, W., Martinson, D., Stammerjohn, S. E., and Schofield, O.: Recent changes in phytoplankton communities associated with rapid regional climate change along the Western Antarctic Peninsula, Science, 323, 1470-1473, 10.1126/science.1164533, 2008.

Moore, C. M., Mills, M. M., Arrigo, K. R., Berman-Frank, I., Bopp, L., Boyd, P. W., Galbraith, E. D., Geider, R. J., Guieu, C., Jaccard, S. L., Jickells, T. D., La Roche, J., Lenton, T. M., Mahowald, N. M., Marañón, E., Marinov, I., Moore, J. K., Nakatsuka, T., Oschlies, A., Saito, M. A., Thingstad, T. F., Tsuda, A., and Ulloa, O.: Processes and patterns of oceanic nutrient limitation, Nature Geoscience, 6, 701-710, 10.1038/NGEO1765, 2013.

Moore, C. M., Seeyave, S., Hickman, A. E., Allen, J. T., Lucas, M. I., Planquette, H., Pollard, R. T., and Poulton, A. J.: Iron-light interactions during the CROZet natural iron bloom and EXport experiment (CROZEX) I: Phytoplankton growth and photophysiology, Deep-Sea Research II, 54, 2045-2065, 10.1016/j.dsr2.2007.06.011, 2007.

Morel, A.: Optical modelling of the upper ocean in relation to its biogenous matter content (case 1 waters), J Geophys Res, 93, 10749-10768, 10.1029/JC093iC09p10749, 1988.

Morel, A., Huot, Y., Gentili, B., Werdell, P. J., Hooker, S. B., and Franz, B. A.: Examining the consistency of products derived from various ocean color sensors in open ocean (Case 1) waters in the perspective of a multi-sensor approach, Remote Sens Environ, 111, 69-88, 10.1016/j.rse.2007.03.012, 2007.

Nicholson, S.-A., Lévy, M., Llort, J., Swart, S., and Monteiro, P. M. S.: Investigating into the impact of storms on sustaining summer primary productivity in the Sub-Antarctic Ocean, Geophysical Research Letters, 43, 10.1002/2016GL069973, 2016.

Nowlin, W. D. and Klinck, J. M.: The physics of the Antarctic Circumpolar Current, Reviews of Geophysics, 24, 469-491, 10.1029/RG024i003p00469, 1986.

Obata, H., Karatani, H., and Nakayama, E.: Automated determination of iron in seawater by chelating resin concentration and chemiluminescence detection, Anal Chem, 65, 1524-1528, 10.1021/ac00059a007, 1993.

Orsi, A. H., Whitworth III, T. W., and Nowlin, W. D.: On the meridional extent and front of the Antarctic Circumpolar Current, Deep-Sea Research I, 42, 641-673, 10.1016/0967-0637(95)00021-W, 1995.

Pakhomov, E. A. and Froneman, P. W.: Zooplankton dynamics in the eastern Atlantic sector of the Southern Ocean during austral summer 1997/1998, Deep-Sea Research II, 51, 2599-2616, 10.1016/j.dsr2.2000.11.001, 2004.

Platt, T., Gallegos, C. L., and Harrison, W. G.: Photoinhibition of photosynthesis in natural assemblages of marine phytoplankton, Journal of Marine Research, 38, 687-701, 1980.

Platt, T. and Sathyendranath, S.: Estimators of primary production for interpretation of remotely-sensed data on ocean colour, J Geophys Res, 98, 14561-14576, 10.1029/93JC01001, 1993.
Platt, T., Sathyendranath, S., and Fuentes-Yaco, C.: Biological oceanography and fisheries management: perspective after 10 years, ICES J Mar Sci, 64, 863-869, 10.1093/icesjms/fsm072, 2007.
Pollard, R. T., Salter, I., Sanders, R. J., Lucas, M. I., Moore, C. M., Mills, R. A., Statham, P. J., Allen, J. T., Baker, A. R., Bakker, D. C. E., Charette, M. A., Fielding, S., Fones, G. R., French, M., Hickman, A. E., Holland, R. J., Hughes, J. A., Jickells, T. D., Lampitt, R. S., Morris, P. J., Nedelec, F. H., Nielsdottir, M., Planquette, H., Popova, E. E., Poulton, A. J., Read, J. F., Seeyave, S., Smith, T., Stinchcombe, M., Taylor, S., Thomalla, S., Venables, H. J., Williamson, R., and Zubkov, M. V.: Southern Ocean deep-water carbon export enhanced by natural iron fertilization, Nature, 457, 577-U581, 10.1038/nature07716, 2009.
Price, N. M., Ahner, B. A., and Morel, F. M. M.: The equatorial Pacific Ocean: Grazer-controlled phytoplankton populations in an iron-limited ecosystem, Limnol Oceanogr, 39, 520-534, 10.4319/lo.1994.39.3.0520, 1994.
Quigg, A., Finkel, Z. V., Irwin, A. J., Rosenthal, Y., Ho, T.-Y., Reinfelder, J. R., Schofield, O., Morel, F. M. M., and Falkowski, P. G.: The evolutionary influence of elemental stoichiometry in marine phytoplankton, Nature, 425, 291-294, 2003.
Ras, J., Claustre, H., and Uitz, J.: Spatial variability of phytoplankton pigment distributions in the Subtropical South Pacific Ocean: comparison between in situ and predicted data, Biogeosciences, 5, 353-369, 10.5194/bg-5-353-2008, 2008.
Raven, J. A.: Predictions of Mn and Fe use efficiencies of phototrophic growth as a function of light availability for growth and C assimilation pathway, New Phytol, 116, 1-18, 10.1111/j.1469-8137.1990.tb00505.x, 1990.
Rio, M. H., Guinehut, S., and Larnicol, G.: New CNES-CLS09 global mean dynamic topography computed from the combination of GRACE data, altimetry, and in situ measurements, J Geophys Res, 116, C07018, 10.1029/2010JC006505, 2011.
Roháček, K.: Chlorophyll Fluorescence Parameters: The Definitions, Photosynthetic Meaning, and Mutual Relationships, Photosynthetica, 40, 13-29, 10.1023/A:1020125719386, 2002.
Ryan-Keogh, T. J., DeLizo, L. M., Smith, W. O., Jr., Sedwick, P. N., McGillicuddy, D. J., Jr., Moore, C. M., and Bibby, T. S.: Temporal progression of photosynthetic strategy by phytoplankton in the Ross Sea, Antarctica, Journal of Marine Systems, 166, 87-96, 10.1016/j.jmarsys.2016.08.014, 2017.
Ryan-Keogh, T. J., Macey, A. I., Nielsdóttir, M., Lucas, M. I., Steigenberger, S. S., Stinchcombe, M. C., Achterberg, E. P., Bibby, T. S., and Moore, C. M.: Spatial and temporal development of phytoplankton iron stress in relation to bloom dynamics in the high-latitude North Atlantic Ocean, Limnol Oceanogr, 58, 533-545, 10.4319/lo.2013.58.2.0533, 2013.
Sathyendranath, S. and Platt, T.: Spectral effects in bio-optical control on the ocean system, Oceanologia, 49, 5-39, 2007.
Schlitzer, R.: Carbon export fluxes in the Southern Ocean: results from inverse modeling and comparion with satellite-based estimates, Deep-Sea Research II, 49, 1623-1644, 10.4319/lo.1994.39.3.0520, 2002.
Sedwick, P. N. and DiTullio, G. R.: Regulation of algal blooms in Antarctic shelf waters by the release of iron from melting sea ice, Geophysical Research Letters, 24, 2515-2518, 10.1029/97GL02596, 1997.
Smetacek, V., Assmy, P., and Henjes, J.: The role of grazing in structuring Southern Ocean pelagic ecosystems and biogeochemical cycles, Antarct Sci, 16, 541-558, 10.1017/S0954102004002317, 2004.

683 Smith, W. O. J. and Donaldson, K.: Photosynthesis-irradiance responses in the Ross Sea, Antartica: a meta-
684 analysis, Biogeosciences, 12, 3567-3577, 10.5194/bg-12-3567-2015, 2015.
685 Strzepek, R. F. and Harrison, P. J.: Photosynthetic architecture differs in coastal and oceanic diatoms, Nature,
686 431, 689-692, 10.1038/nature02954, 2004.
687 Strzepek, R. F., Hunter, K. A., Frew, R. D., Harrison, P. J., and Boyd, P. W.: Iron-light interactions differ in
688 Southern Ocean phytoplankton, Limnol Oceanogr, 57, 1182-1200, 10.4319/lo.2012.57.4.1182, 2012.
689 Sunda, W. G. and Huntsman, S. A.: Interrelated influence of iron, light and cell size on marine phytoplankton
690 growth, Nature, 390, 389-392, 10.1038/37093, 1997.
691 Swart, S., Chang, N., Fauchereau, N., Joubert, W., Lucas, M., Mtshali, T., Roychoudhury, A., Tagliabue, A.,
692 Thomalla, S., Waldron, H., and Monteiro, P. M. S.: Southern Ocean Seasonal Cycle Experiment 2012: Seasonal
693 scale climate and carbon cycle links, S Afr J Sci, 108, 11-13, 10.4102/sajs.v108i3/4.1089, 2012.
694 Swart, S., Speich, S., Ansorge, I. J., and Lutjeharms, J. R. E.: An altimetry-based gravest empirical mode south
695 of Africa: 1. Development and validation, J Geophys Res, 115, C03002, 10.1029/2009JC005299, 2010.
696 Swart, S., Thomalla, S. J., and Monteiro, P. M. S.: The seasonal cycle of mixed layer dynamics and
697 phytoplankton biomass in the Sub-Antarctic Zone: A high-resolution glider experiment, Journal of Marine
698 Systems, 147, 103-115, 10.1016/j.jmarsys.2014.06.002, 2015.
699 Tagliabue, A., Sallée, J.-B., Bowie, A. R., Lévy, M., Swart, S., and Boyd, P. W.: Surface-water iron supplies in
700 the Southern Ocean sustained by deep winter mixing, Nature Geoscience, 7, 314-320, 10.1038/ngeo2101, 2014.
701 Thomalla, S. J., Fauchereau, N., Swart, S., and Monteiro, P. M. S.: Regional scale characteristics of the seasonal
702 cycle of chlorophyll in the Southern Ocean, Biogeosciences, 8, 2849-2866, 10.5194/bg-8-2849-2011, 2011.
703 Thomalla, S. J., Racault, M.-F., Swart, S., and Monteiro, P. M. S.: High-resolution view of the spring bloom
704 initiation and net community production in the Subantarctic Southern Ocean using glider data, ICES J Mar Sci,
705 72, 1999-2020, 10.1093/icesjms/fsv105, 2015.
706 Twining, B. S. and Baines, S. B.: The trace metal composition of marine phytoplankton, Annual Review of
707 Marine Science, 5, 191-215, 10.1146/annurev-marine-121211-172322, 2013.
708 Welschmeyer, N. A.: Fluorometric analysis of chlorophyll-*a* in the presence of chlorophyll-b and pheopigments,
709 Limnol Oceanogr, 39, 1985-1992, 10.4319/lo.1994.39.8.1985, 1994.
710 Wolters, M.: Quickchem Method 31-114-27-1-D - Silicate in Brackish or Seawater, Lachat Instruments, 2002.
711 Zhang, J. L.: Increasing Antarctic sea ice under warming atmospheric and oceanic conditions, Journal of
712 Climate, 20, 2515-2529, 10.1175/jcli4136.1, 2007.
713

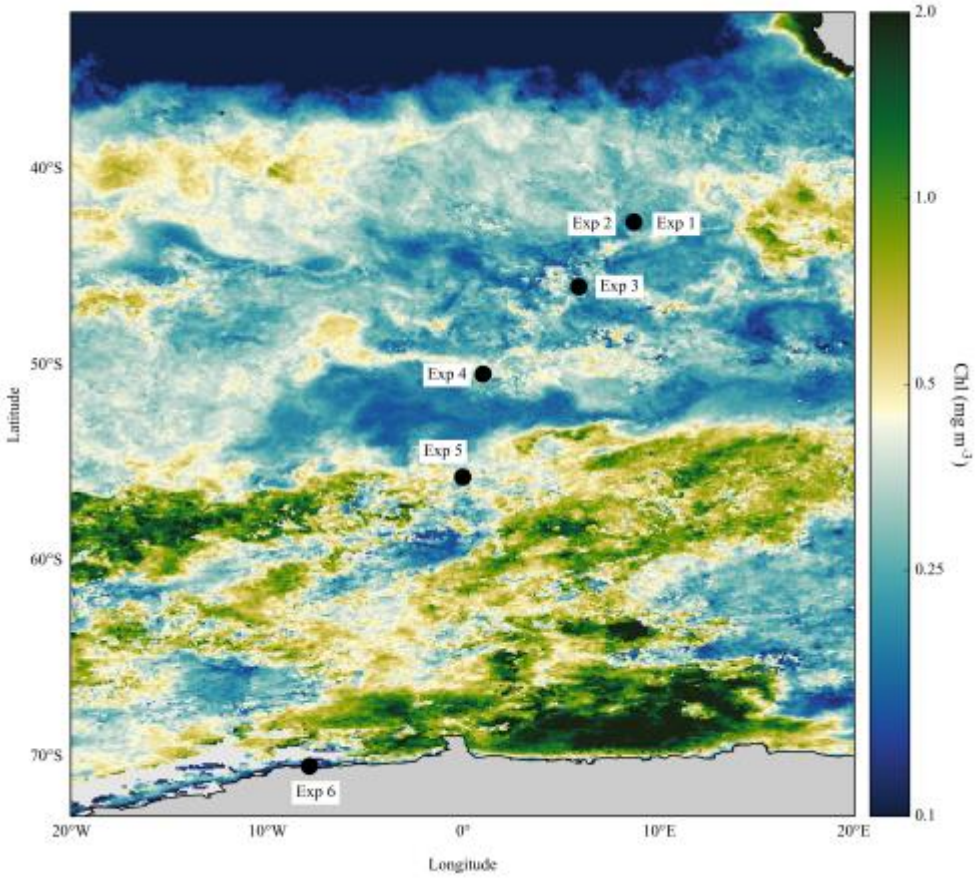

714

715 **Figure 1: Composite map of MODIS (8-day, 9 km) derived chlorophyll (mg m^{-3}) from November 2015 to March 2016**
716 **for the Atlantic sector of the Southern Ocean with locations of the nutrient addition productivity versus irradiance**
717 **(PE) experiments.**

718

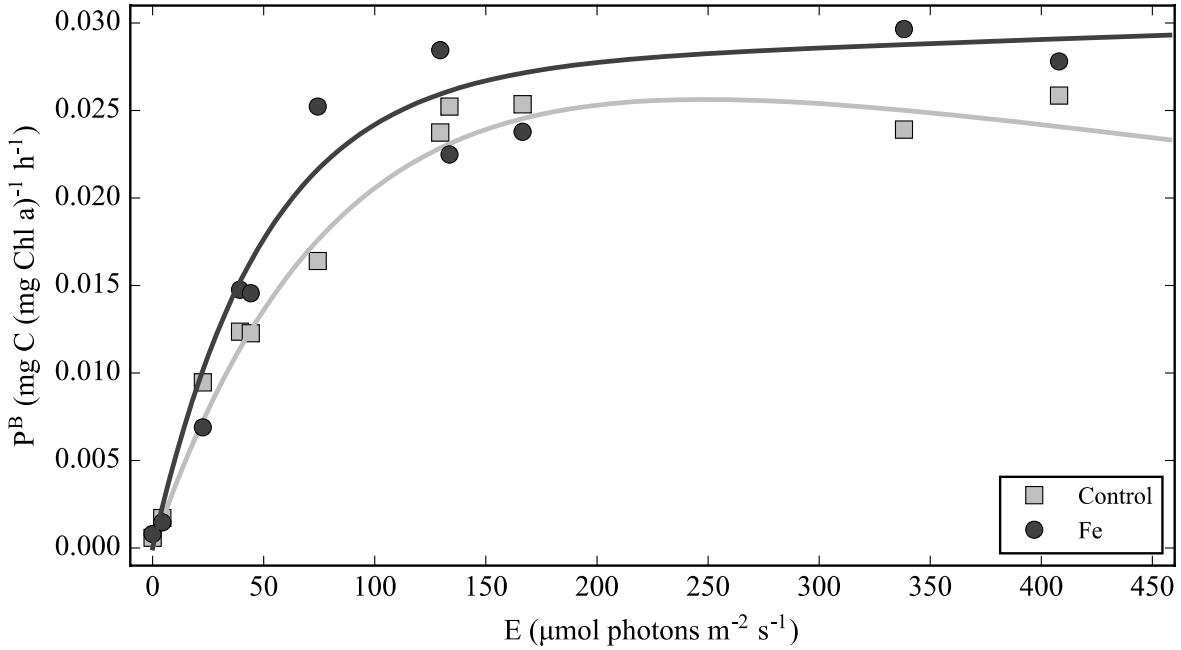

Figure 2: An example of a PE curve of productivity (mg C (mg Chl a)$^{-1}$ h^{-1}), versus irradiance (µmol photons m^{-2} s^{-1}), with (Fe) and without (Control) the addition of iron; the lines represent a non-linear least squares fit to the equation of Platt et al. (1980).

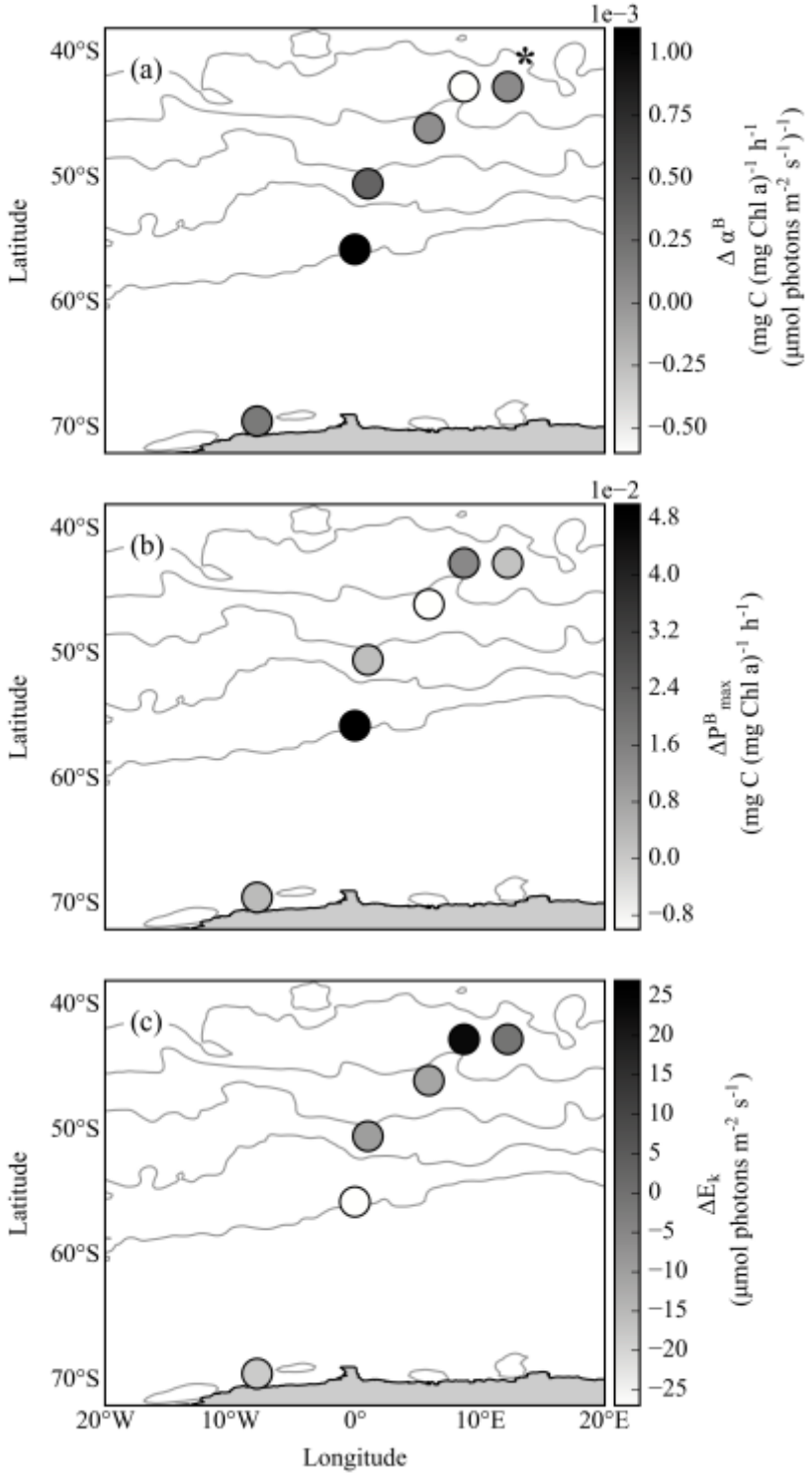

Figure 3: Experimental values of (a) $\Delta\alpha^B$ (mg C (mg Chl a)$^{-1}$ h^{-1} (µmol photons m^{-2} s^{-1})$^{-1}$), (b) ΔP^B_{max} (mg C (mg Chl a)$^{-1}$ h^{-1}) and (c) ΔE_k (µmol photons m^{-2} s^{-1}) for experiments set up in the Atlantic sector of the Southern Ocean. Ocean fronts, indicated by grey lines, were determined from MADT from the CLS/AVISO product (Rio et al., 2011) and their position averaged over 5 months (November 2015 to March 2016). From north – south: Sub-Tropical Front (STF), Sub-Antarctic Front (SAF), Antarctic Polar Front (APF), Southern Antarctic Circumpolar Front (SACCF) and the Southern Boundary (SBdy). *Position of experiment 3 moved 2.5° eastwards for presentation purposes.

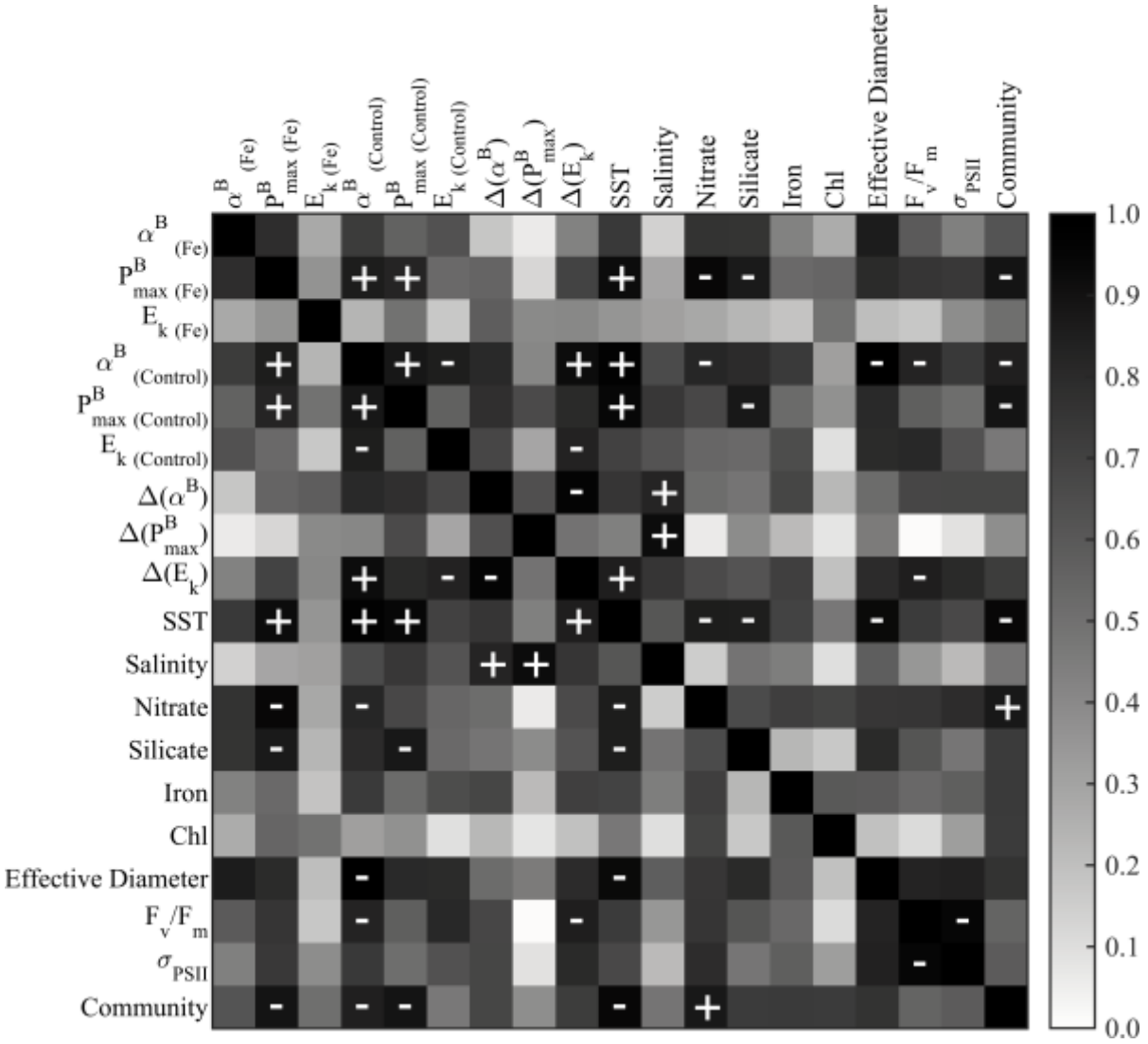

Figure 4: Matrix of Pearson's linear correlation coefficients between the photosynthetic parameters determined experimentally and *in situ* variables measured, including: α^B, P^B_{max} and E_k from the both Fe and control treatments, the relative differences, sea surface temperature (SST), Salinity, Nitrate, Silicate and dissolved Iron concentration, Chl concentration, Effective Diameter, F_v/F_m, σ_{PSII} and Community composition (ratio of Diatoms to Haptophytes). The strength of the linear relationship associated between each pair of variables is indicated by the colour of the square, with the negative and positive correlations denoted by '-' and '+' within all squares where significant ($p<0.05$).

744 Figure 5

745

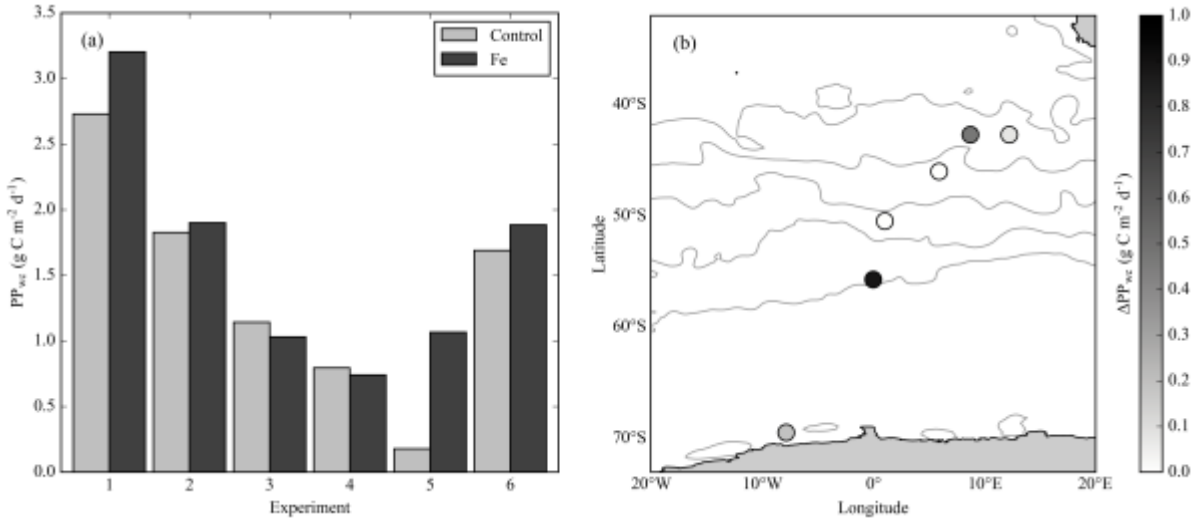

746

747 **Figure 5: Modelled outputs of primary production utilizing experimentally derived photosynthetic parameters. (a)**
748 **Depth integrated primary production (PP_{wc}) (mg C m^{-2} d^{-1}) and (b) ΔPP_{wc} (mg C m^{-2} d^{-1}). Ocean fronts, indicated by**
749 **grey lines, displayed as in Fig. 3.**

750

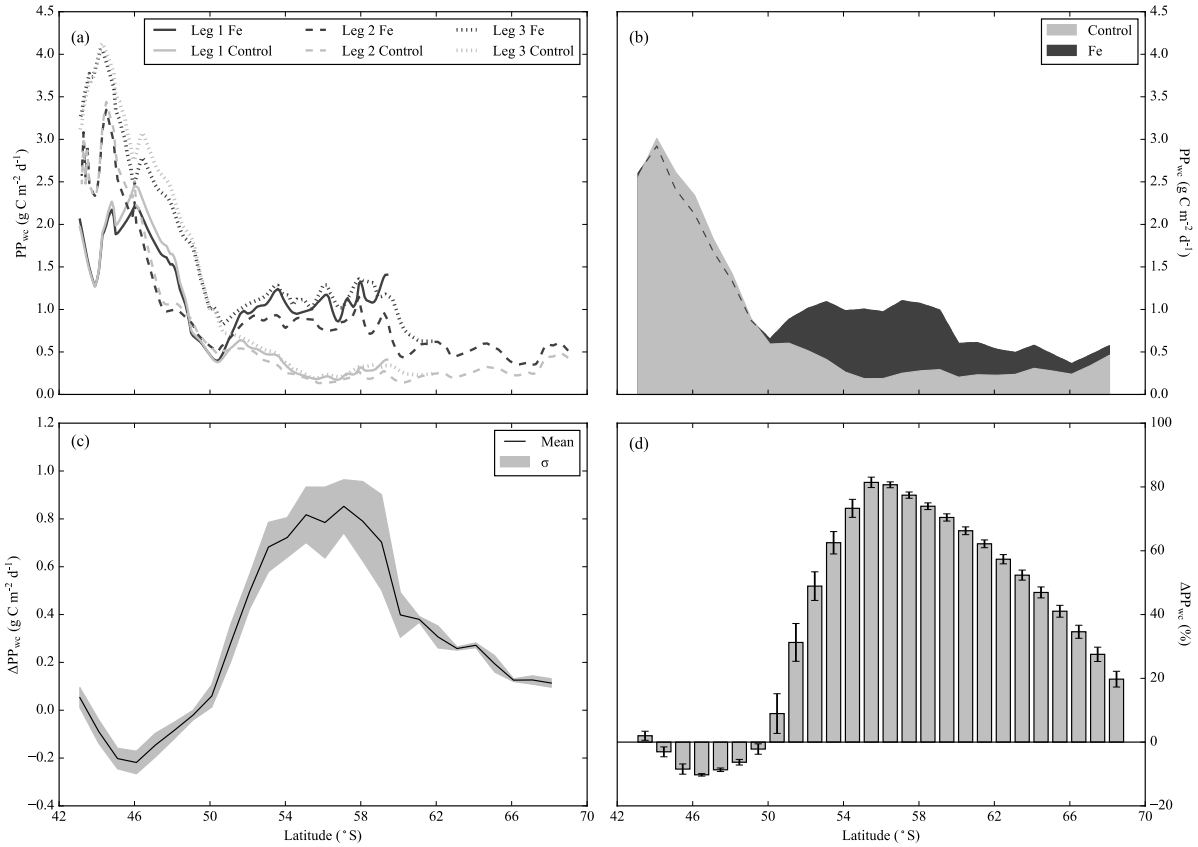

Figure 6: Depth integrated primary production (PP_{wc}) (mg C m^{-2} d^{-1}) for each transect (Leg 1 -3) (a) interpolated along the transect line utilizing linearly interpolated values for α and P_{max} as determined from the Fe and Control treatments. (b) Mean PP_{wc} (mg C m^{-2} d^{-1}) with ± standard deviation (σ). (c) The mean absolute differences in PPwc (ΔPP_{wc}) with ± standard deviation between the Fe and Control treatments. (d) ΔPP_{wc} represented as the mean percentage difference with ± standard deviations.

759

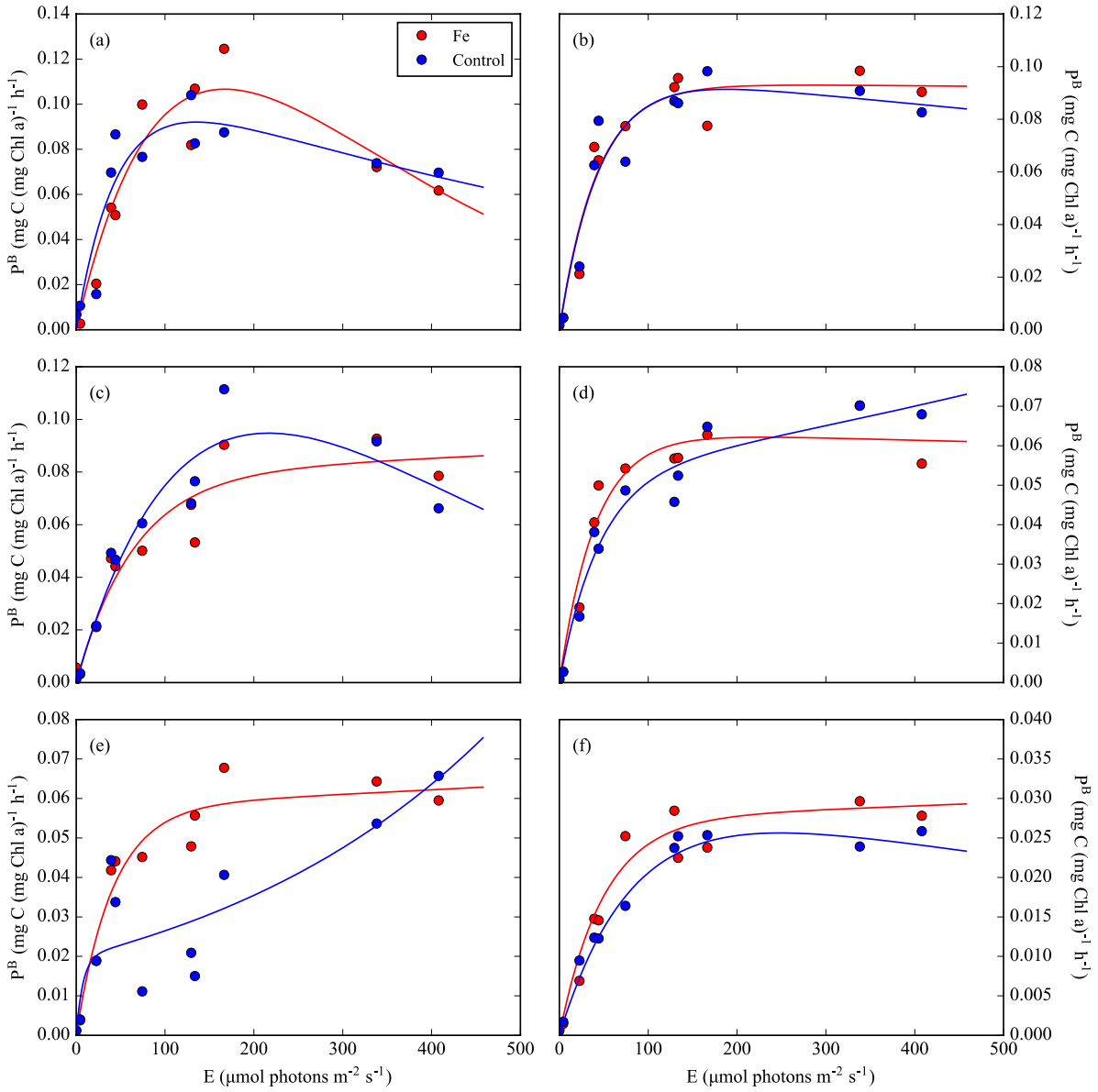

760

761 **Figure S1: PE curves of productivity (mg C (mg Chl a)$^{-1}$ h^{-1}) with (Fe, red dots) and without (Control, blue dots) the**
762 **addition of iron for experiments (a) 1, (b) 2, (c) 3, (d) 4, (e) 5 and (f) 6; lines represent a non-linear least squares fit to**
763 **the equation of Platt et al. (1980).**

764

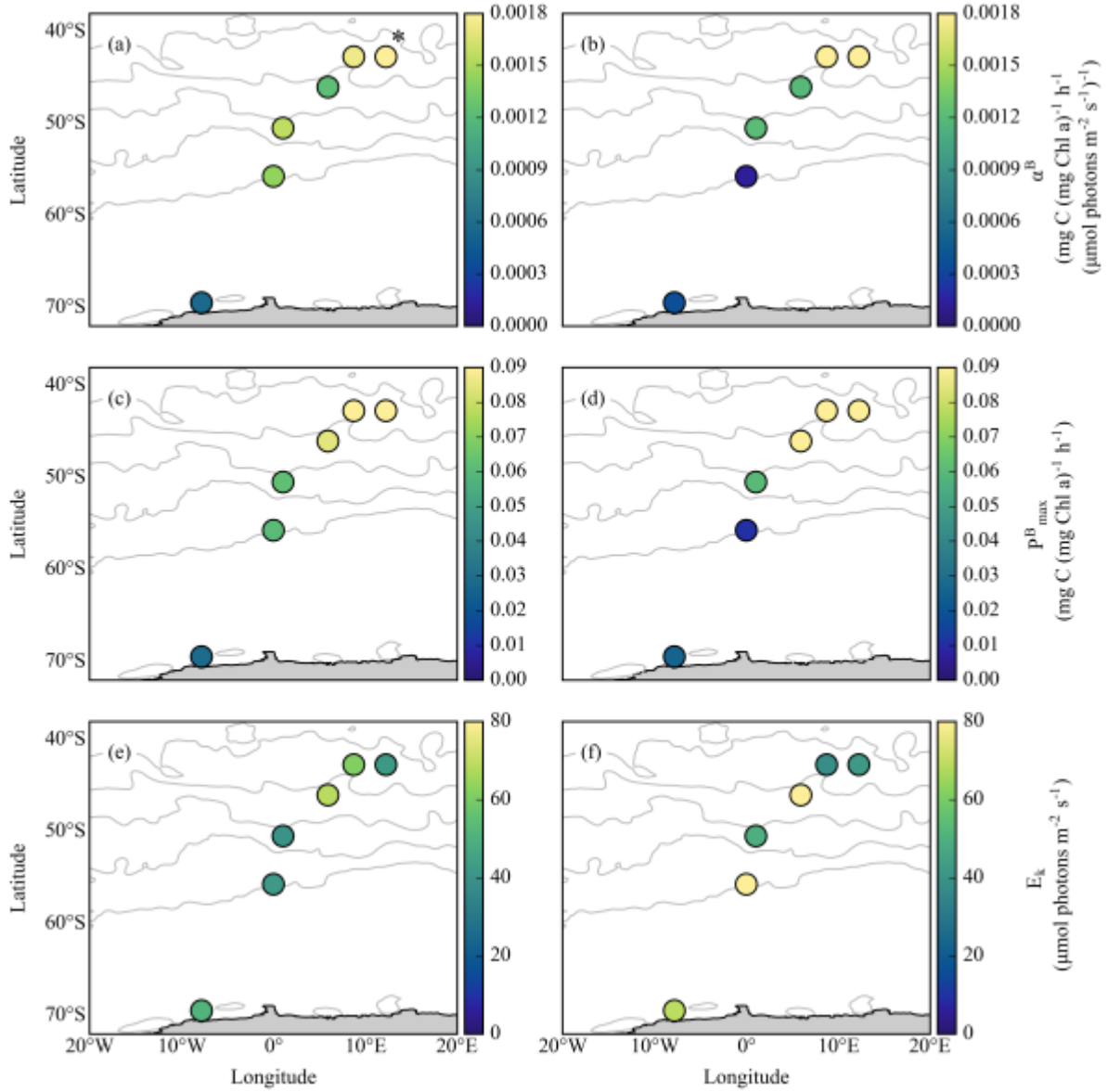

Figure S2: PE parameters (a) α^B (mg C (mg Chl a)$^{-1}$ h^{-1} (µmol photons m^{-2} s^{-1})$^{-1}$), (b) P^B_{max} (mg C (mg Chl a)$^{-1}$ h^{-1}) and (c) E_k (µmol photons m^{-2} s^{-1}) for the iron addition and control treatments of experiments set up in the Atlantic sector of the Southern Ocean.

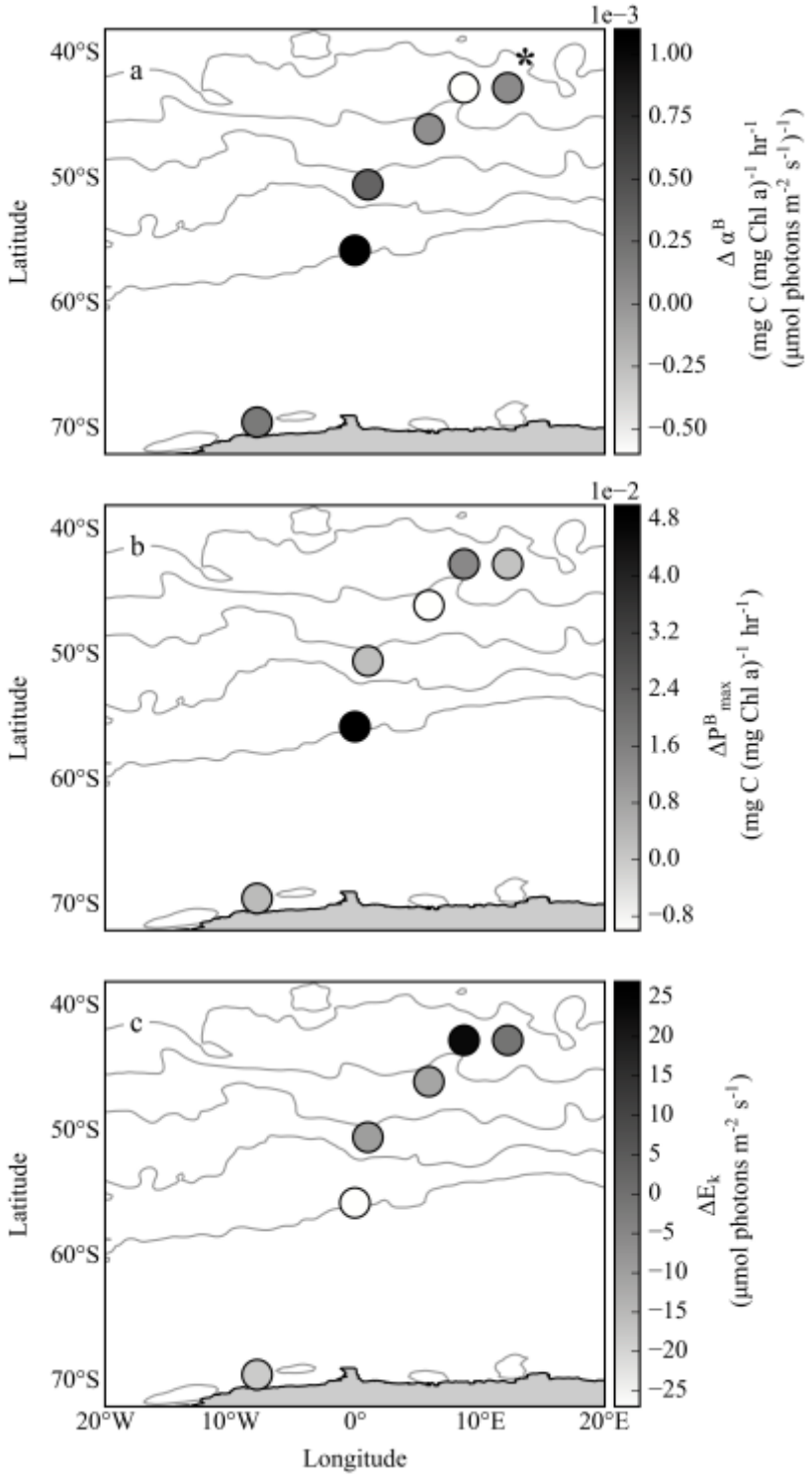

771
772

773 **Figure S3: Absolute differences in the PE parameters between the iron treatment and the control**
774 **treatment (a) α^B (mg C (mg Chl a)$^{-1}$ h^{-1} (µmol photons m^{-2} s^{-1})$^{-1}$), (b) P^B_{max} (mg C (mg Chl a)$^{-1}$ h^{-1}) and (c) E_k (µmol**
775 **photons m^{-2} s^{-1}) for experiments set up in the Atlantic sector of the Southern Ocean.**

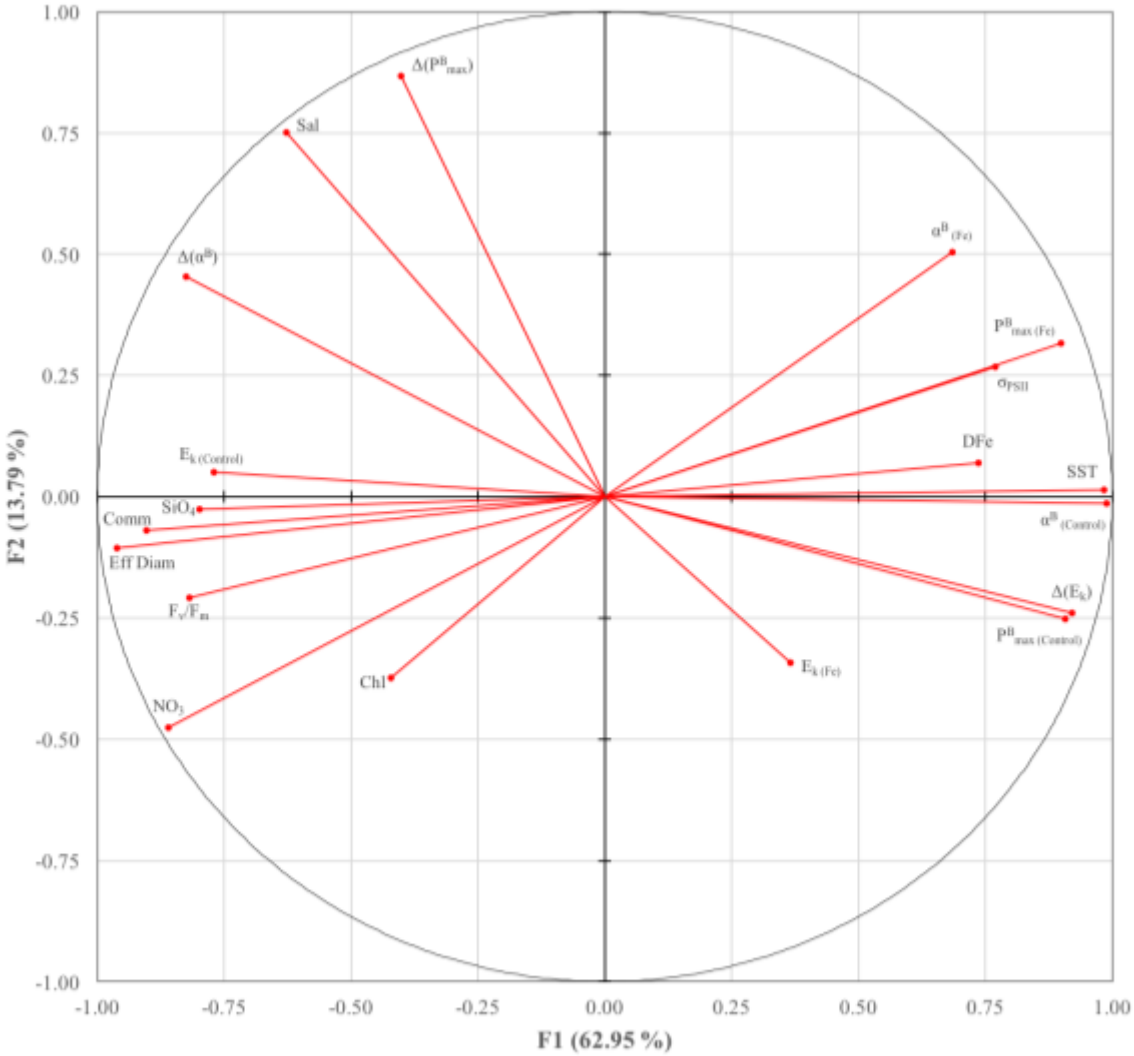

Figure S4: PCA: projection of the photosynthetic parameters determined experimentally and *in situ* variables measured, including: α^B, P^B_{max} and E_k from the both Fe and control treatments, the relative differences, sea surface temperature (SST), Salinity, Nitrate, Silicate and dissolved Iron concentration, Chl concentration, Effective Diameter, F_v/F_m, σ_{PSII} and Community composition (ratio of Diatoms to Haptophytes).

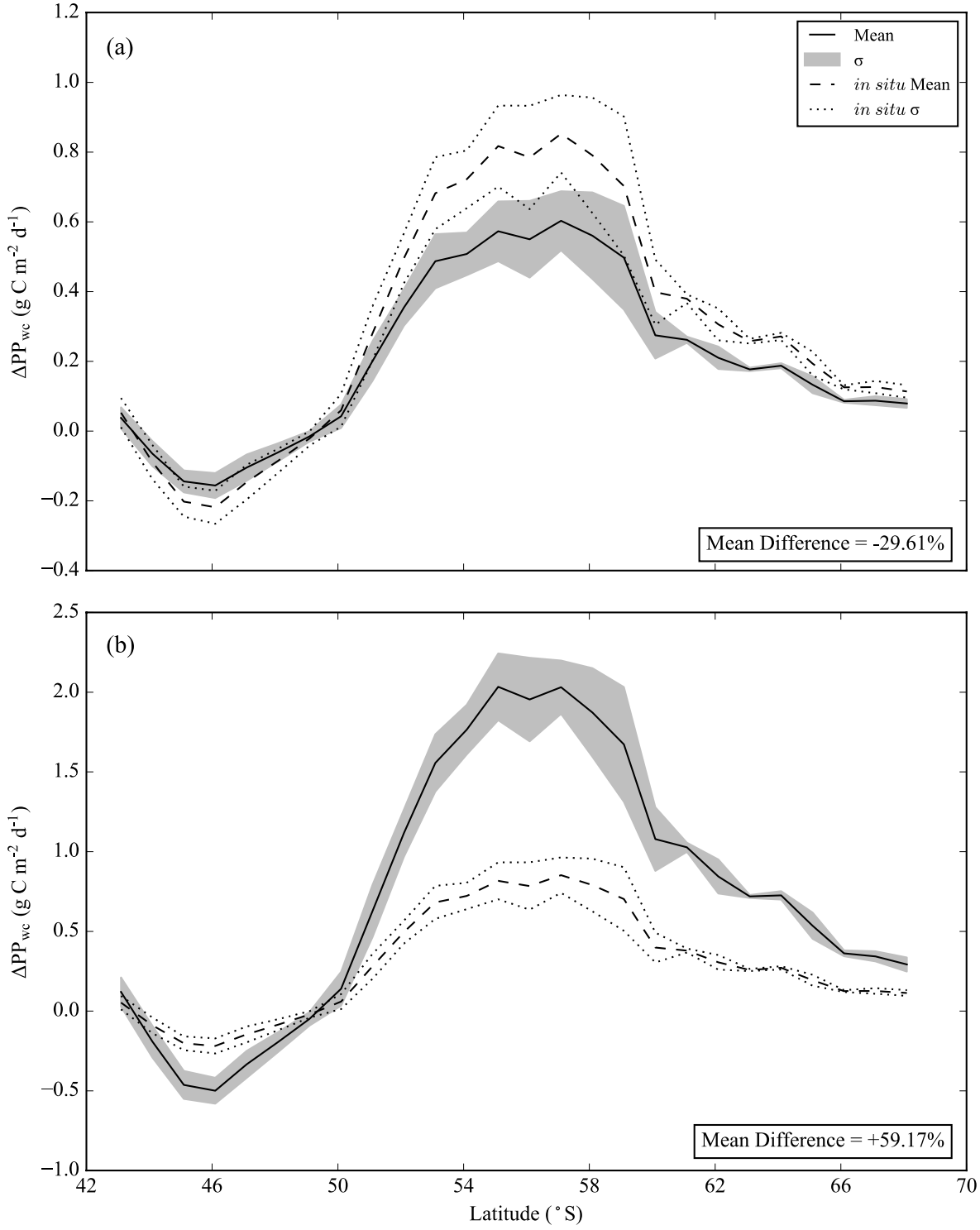

Figure S5: The absolute mean differences in depth integrated primary production (ΔPP_{wc}) with ± standard deviation (σ) interpolated along the transect line utilizing the (a) increased K_d values and (b) decreased K_d values; also displayed is PP_{wc} derived utilizing *in situ* K_d.

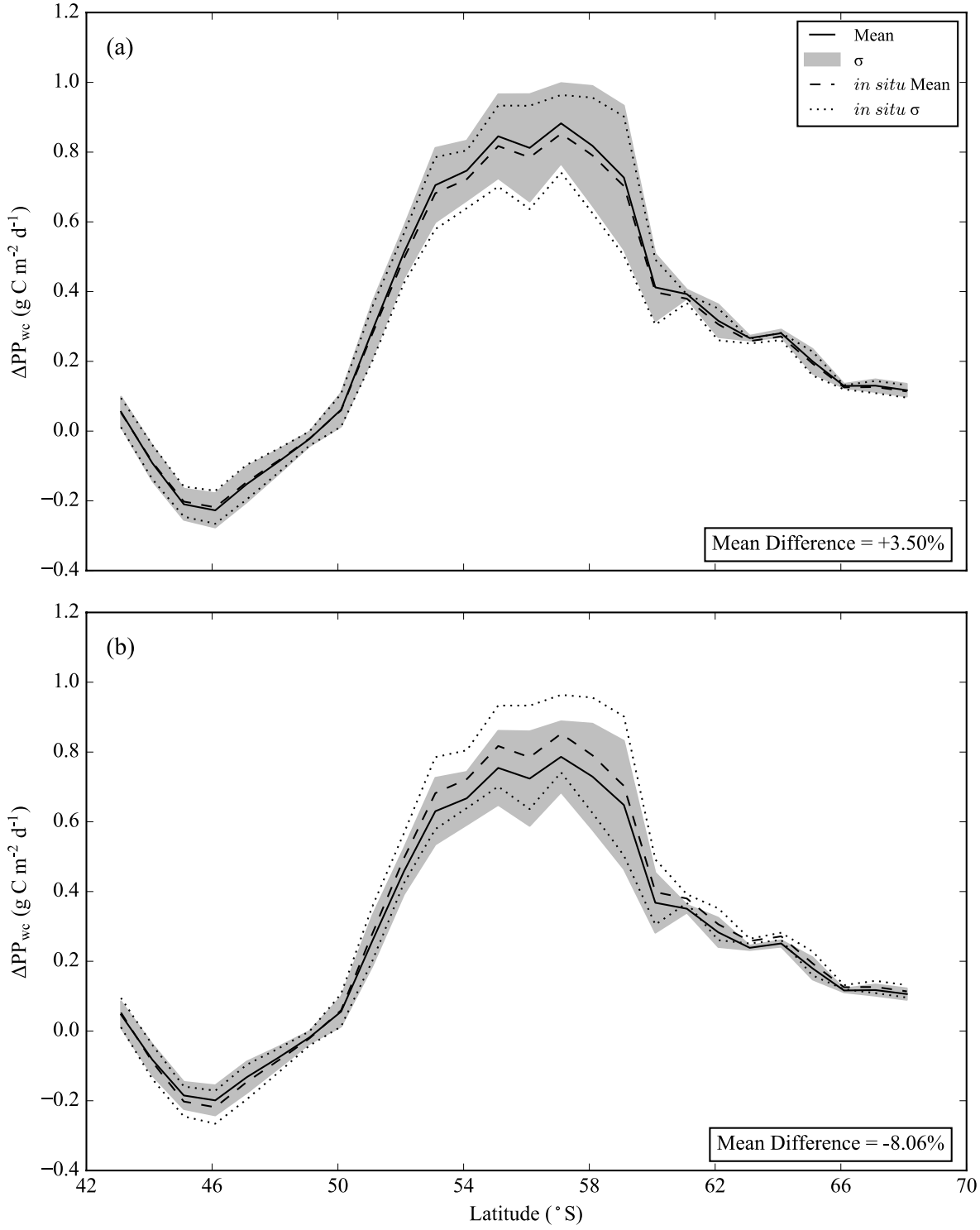

Figure S6: The absolute mean differences in depth integrated primary production (ΔPP_{wc}) with ± standard deviation (σ) interpolated along the transect line utilizing the (a) increased PAR values and (b) decreased PAR values; also displayed is PP_{wc} derived utilizing *in situ* PAR.

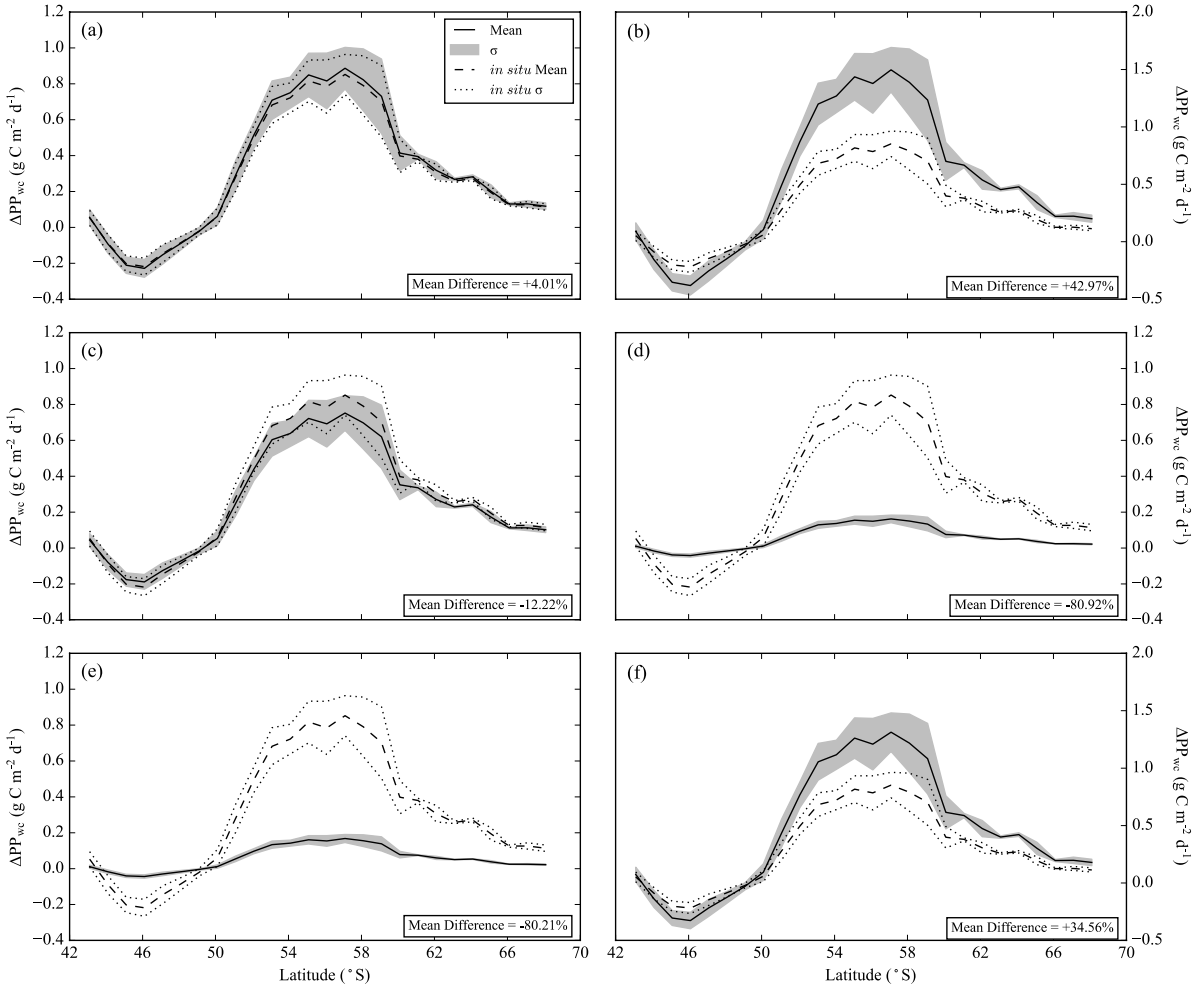

Figure S7: The absolute mean differences in depth integrated primary production (ΔPP_{wc}) with ± standard deviation (σ) interpolated along the transect line utilizing increased (a) α values and (b) P_{max} values, decreased (c) α values and (d) P_{max} values, (e) increase α and decreased P_{max} values and (f) decreased α and increased P_{max} values. Displayed on all plots is the PP_{wc} derived utilizing the *in situ* α and P_{max} values. (Please note the different scales in subplots b & f).